Biophysical Journal Volume 74 April 1998 1658–1676

Computation of the Internal Forces in Cilia: Application to Ciliary Motion, the Effects of Viscosity, and Cilia Interactions

Shay Gueron and Konstantin Levit-Gurevich
Department of Mathematics, Technion-Israel Institute of Technology, Haifa 32000, Israel

ABSTRACT This paper presents a simple and reasonable method for generating a phenomenological model of the internal mechanism of cilia. The model uses a relatively small number of parameters whose values can be obtained by fitting to ciliary beat shapes. Here, we use beat patterns observed in *Paramecium*. The forces that generate these beats are computed and fit to a simple functional form called the "engine." This engine is incorporated into a recently developed hydrodynamic model that accounts for interactions between neighboring cilia and between the cilia and the surface from which they emerge. The model results are compared to data on ciliary beat patterns of *Paramecium* obtained under conditions where the beats are two-dimensional. Many essential features of the motion, including several properties that are not built in explicitly, are shown to be captured. In particular, the model displays a realistic change in beat pattern and frequency in response to increased viscosity and to the presence of neighboring cilia in configurations such as rows of cilia and two-dimensional arrays of cilia. We found that when two adjacent model cilia start beating at different phases they become synchronized within several beat periods, as observed in experiments where two flagella are brought into close proximity. Furthermore, examination of various multiciliary configurations shows that an approximately antiplectic wave pattern evolves autonomously. This modeling evidence supports earlier conjectures that metachronism may occur, at least partially, as a self-organized phenomenon due to hydrodynamic interactions between neighboring cilia.

INTRODUCTION

This paper deals with modeling the internal forces that produce ciliary motion, the changes of ciliary beats in response to changes in the viscosity of the surrounding fluid, and the investigation of cilia interactions. We are particularly interested in the formation of metachronal waves, phenomena which have attracted a great deal of research effort both experimentally and theoretically.

Metachronal coordination between cilia is a situation where cilia beat together with a constant phase difference between adjacent neighbors and their tips form a moving wave pattern. Metachronal waves appear in various forms, depending on the direction of the wave propagation. Symplectic metachronism is the case where the wave propagates in the direction of the effective stroke [for example, the cilia of *Opalina* (Sleigh, 1962)]. When the wave propagates in a direction opposite to that of the effective stroke, the metachronism is called antiplectic. Diaplectic metachronism is the case where the direction of the metachronal wave is perpendicular to the direction of the effective stroke. In some cases cilia can change the type of their metachronism in response to changes in the environment, such as changed fluid viscosity, as observed with the cilia of *Paramecium* by Machemer (1972). The reason why and how arrays of cilia beat in a metachronal pattern is not fully understood. The work of Machemer (1972), for example, shows that membrane voltage and calcium levels affect the direction of the metachronal wave as well as the directions of the effective and the recovery strokes of the cilia. On the other hand, some researchers have speculated that metachronism may result from hydrodynamical coupling (e.g., Sleigh, 1974; Gheber and Priel, 1989). The work we present here provides a theoretical model that partially supports this conjecture.

The motion of cilia and flagella is governed by the Stokes equations with no-slip boundary conditions on their surfaces and vanishing fluid disturbance at infinity. The slenderness of cilia/flagella justifies certain asymptotic approximations used to relate the local drag forces to the local velocity. This approach, which was pioneered by Gray and Hancock (1955) (referred to as G-H hereafter), assumes that the tangential, normal, and binormal components of the drag force are proportional to the respective components of the velocity, with different proportionality constants. The G-H approximation has been used extensively in many models because of its simple implementation. However, it has severe limitations [see, e.g., Lighthill (1975, 1976) and Childress (1981)]. Modifications of the drag coefficients, known as resistive force theories (RFT), were tried as an attempt to overcome these problems (Lighthill, 1975; Brennen and Winet, 1977; Johnson and Brokaw, 1979). Unfortunately, the RFT was not accurate enough, for example in the case of the flagellum with an attached cell body (Johnson and Brokaw, 1979). Furthermore, even if one could somehow obtain resistance coefficients that are accurate for modeling the motion of a single cilium, there is no justification for its use in cases where the cilium moves in external flows, since these coefficients depend on such flows. Also, there is no reason to believe that they would remain constant along the cilium at all times under such conditions. Thus, RFT is not

Received for publication 2 April 1997 and in final form 24 November 1997.
Address reprint requests to Dr. Shay Gueron, Dept. of Mathematics, Technion-Israel Institute of Technology, Haifa 32000, Israel. Tel.: 972-4-8294092; Fax: 972-4-8324654; E-mail: shay@math.technion.ac.il.
K. Levit-Gurevich's E-mail address is konstant@math.technion.ac.il.

0006-3495/98/04/1658/19 $2.00

applicable for modeling multicilia configurations. A more consistent method to relate the drag forces and the velocity through a vectorial integral equation for the drag forces was suggested by Lighthill (1976) and proved by Childress (1981). Lighthill's equation is an integral equation of the first kind with respect to its tangential component and is therefore ill-posed. In addition, its integrand is singular and the integration interval contains points that are close to the singularity. This introduces severe problems in any attempt at a numerical solution. Other hydrodynamic analyses, generally referred to as slender body theory, have been developed and refined by many authors. They were applied to various problems involving flagellar motion, offering different methods to relate between the drag forces and the velocities (Johnson and Brokaw, 1979; Dresdner et al., 1980; Higdon, 1979a–c; Phan-Thien et al., 1987; Myerscough and Swan, 1989; Ramia, 1991). In a recent publication, Gueron and Liron (1992) (GL hereafter) presented a method that overcomes the above difficulties. They introduced a variation on Lighthill's equation that yields a well-posed integral equation of the second kind for the normal, tangential, and binormal drag forces, thus keeping the integration interval away from the singularity. This improved the accuracy and consistency of the model for cilia beating. More important, the GL equations are the first published method for dynamical simulations of multicilia configurations that account for the effects of neighboring cilia and the effect of the surface from which the cilia emerge. This model was originally applied to a two-dimensional setup and later extended to describe three-dimensional beating (Gueron and Liron, 1993).

Modeling the internal mechanism of cilia is a very challenging problem, and no satisfactory model has been developed so far. We review here briefly some of the previous modeling attempts, discussing the involved difficulties.

The work of GL was mainly oriented toward developing a framework that facilitates dynamical modeling of multicilia configurations. To describe the internal mechanism of the cilia (hereafter referred to as the "engine") phenomenologically, they used an ad-hoc equation that represented the active normal shear force generated inside a cilium. The GL engine included a built-in frequency term that controlled the resulting beat frequency and predetermined the duration of the effective and the recovery strokes. Therefore, this model engine does not allow for realistic changes in the beat frequency in response to changed external load such as increased viscosity or external flow generated by neighboring cilia. This is also the reason why it is not appropriate for investigating metachronism. In the GL modeling framework the engine part is kept as a separate building block, which can be readily replaced by a more realistic version, as we demonstrate in this paper.

Experiments show that when flagella are pinned at one end to a flat surface they tend to change their beat pattern from a symmetric cycle (which is typical for flagella) to an asymmetric beat pattern similar to that of cilia [see, for example, Blum and Hines (1979)]. Inspired by these results and the similarity between the internal structure of cilia and flagella, Blum and Hines (1979) incorporated ciliary boundary conditions into a model for the motion of flagella. Using a curvature-controlled model (Hines and Blum, 1978) and a self-oscillatory model (Hines and Blum, 1979) they found that a 10-μm-long model cilium did not move at all with a flagellar engine, while a longer model cilium moved with a symmetric beat pattern similar to flagella. Thus, they could not obtain a ciliary beat pattern by simply changing the boundary conditions in a flagellar motion model. Obviously, some other factors are responsible for the asymmetric patterns.

Excitable dynein models for the internal engine of cilia and flagella were suggested in a series of papers by Murase and Shimizu (1986), Murase et al. (1989), and Murase (1990, 1991). These models assumed that dynein is normally at a resting position and is activated when the sliding exceeds some threshold value. These models were tested only under the assumption of small amplitude motion, which is not the case for real cilia, and were based on the G-H approximation that is not adequate for modeling multicilia configurations. Also, we found that Murase's model engine (Murase, 1990) gives poor results when incorporated into the GL model.

In the present study we propose a consistent method for calculating the internal forces that generate an observed ciliary motion. To avoid the need for a detailed analysis of the internal filaments, the dynein arms, radial spokes system, and microtubules (see Brokaw, 1985), we model the computed forces by a simple and plausible functional form. The resulting engine represents merely a phenomenological description. To obtain realistic values for the relatively small number of parameters on which our model depends, we use data from observed cilia and compute locations and velocities during the beat cycle. We then solve the GL equations and compute the drag forces, from which we compute the internal shear forces. These forces are used to determine the engine parameters. The transitions from the effective to the recovery stroke and vice versa are modeled by two switches that are controlled by the momentary geometrical configuration. These configuration-dependent switches implicitly reflect the load dependence of the internal engine without using an explicit frequency term in the model engine.

The new engine is tested by incorporating it into the GL dynamical equations for two-dimensional beats. The model produces realistic beats. It also reproduces experimental results such as logarithmic decrease in beat frequency with increased viscosity, self-synchronization between two adjacent cilia, and frequency matching with the frequency of external flows. Finally, we investigate multicilia configurations and obtain dynamic self-synchronization between two adjacent cilia, and phase lags that resemble antiplectic metachronal patterns that evolve autonomously due to the hydrodynamical interaction between the cilia. A brief summary of a portion of this work, without any of the

mathematical and computational details, is presented by Gueron et al. (1997).

THE MODEL EQUATION OF MOTION

Notations

We adopt the notations used by GL and by Hines and Blum (1978). The cilium is considered as an inextensible cylindrical filament of length L and radius a, whose centerline is a curve parameterized by its arclength parameter $0 \le s \le L$. For the two-dimensional motion, the location of each point $[x(s, t), y(s, t)]$ along the cilium, at time t, is determined by the angle $\alpha(s, t)$ between the tangent to the curve and a fixed horizontal axis by the equations

$$x(s, t) = \int_0^s \cos[\alpha(\xi, t)]d\xi, \qquad y(s, t) = \int_0^s \sin[\alpha(\xi, t)]d\xi. \tag{1}$$

The curvature $\kappa = \kappa(s, t)$ satisfies $\kappa = \alpha_s$. We use $\mathbf{F}(s, t)$ to denote the shear force developed by the internal mechanism of the cilium and $\mathbf{M}(s, t)$ for the bending moment it produces. $\phi(s, t)$ is the drag force per unit length, exerted on the cilium by the surrounding fluid of viscosity μ.

The subscripts T and N denote the tangential and normal components of vectors, respectively, and the subscripts s and t denote partial differentiation with respect to the arclength s and to time t, respectively. In general, all locations and forces depend on t and s, but we avoid writing this dependence explicitly whenever it is clear from the context.

Drag force-velocity relation and geometric equations

The hydrodynamic description of cilia motion we use in this work was developed by GL. The drag force-velocity relation is written as

$$\phi_N = -C_N V_N + g_N, \quad \phi_T = -C_T V_T + g_T. \tag{2}$$

where

$$g_N = C_N G_N, \quad g_T = C_T G_T, \tag{3}$$

and $\mathbf{G} = (G_T, G_N)$ is defined by

$$\mathbf{G}(s_0, t) = \int_{|s-s_0|>q} \mathbf{U}_s(r(s_0, t), r(s, t), -\phi(s, t))ds + \int_{0\le s\le L} \{\mathbf{V}_{si}(r(s_0, t), r(s, t), -\phi(s, t)) + \mathbf{V}_{di}(r(s_0, t), r(s, t), -(a^2/4\mu)\phi(s, t))\}ds + \int_{\substack{0\le s\le L \\ \text{neighboring cilia}}} \mathbf{U}_s(r(s_0, t), r(s, t), -\phi(s, t))ds, \tag{4}$$

$$C_T = \frac{8\pi\mu}{-2 + 4\ln(2q/a)}, \quad C_N = \frac{8\pi\mu}{1 + 2\ln(2q/a)}. \tag{5}$$

Here q can take any value such that $q/L \ll 1$, $a/q \ll 1$. The terms that appear as integrands in Eq. 4 are the appropriate singular solutions of the Stokes equation (stokeslets and doublets with and without the image system). Equation 4 is an approximation to order $O(\sqrt{a/L})$. It can generally be used for 3-d motion, but is applied here to planar motions (for more details see GL).

The balance of forces and moments and the equations that relate the components of the velocity to the cilium's geometry (see Lubliner, 1973; Hines and Blum, 1978) are

$$\phi_N = F_{N_s} + F_T\alpha_s, \quad \phi_T = F_{T_s} - F_N\alpha_s, \quad M_s = F_N, \tag{6}$$

$$V_{N_s} = \alpha_t - V_T\alpha_s, \quad V_{T_s} = V_N\alpha_s. \tag{7}$$

F_N, the normal component of the shear force developed within the cilium, is represented by

$$F_N = E_b\alpha_{ss} + S. \tag{8}$$

The first term of Eq. 8 accounts for the elastic stiffness of the cilium and the second term represents the internal engine; that is, the active shear force generated inside the cilium by the sliding filaments mechanism.

Using Eqs. 2, 6, and 7 and the normalized variables $s^* = s/L$, $t^* = w_0 t$, $S^* = S/S_0$ we obtain the following nondimensional equations (written without the asterisks for convenience):

$$F_{T_{ss}} = (1 + C_{TN})F_{N_s}\alpha_s + C_{TN}F_T(\alpha_s)^2 + F_N\alpha_{ss} - C_{TN}g_N\alpha_s + g_{T_s}, \tag{9}$$

$$F_{N_{ss}} + (1 + C_{NT})F_{T_s}\alpha_s + F_T\alpha_{ss} = -(C_N w_0 L^2/S_0)\alpha_t + C_{NT}F_N(\alpha_s)^2 + C_{NT}g_T\alpha_s + g_{N_s}, \tag{10}$$

where $C_{TN} \equiv C_T/C_N$ and $C_{NT} \equiv C_N/C_T$, and $0 \le s \le 1$. For brevity we define $C_N = C_N L^2/S_0$. The values of L, S_0, and w_0 are displayed in Table 1. The nondimensional form of Eq. 8 becomes

$$F_N = \frac{E_b}{S_0 L^2}\cdot\alpha_{ss} + S. \tag{11}$$

The motion of the cilium can be computed from Eqs. 9–11. If a model for $S(s, t)$ is chosen, one can compute F_N from Eq. 11. Then, F_T is determined from Eq. 9 and $\alpha(s, t)$ can be propagated in time by means of Eq. 10. Fig. 1 represents the simulation algorithm for the numerical tech-

TABLE 1 Parameter values for the ciliary motion model

Parameter	Value	Reference
L	12 μm	The length of the cilium of *Paramecium* (Sleigh, 1962)
a	0.1 μm	Typical cilia radius (Sleigh, 1962)
q	1 μm	Gueron and Liron, 1992
w_0	28 beats/s	Typical beat frequency of *Paramecium* (Sleigh, 1962)
S_0	10^{-12} N	Gueron and Liron, 1992
E_b	$25 \cdot 10^{-24}$ N/m^2	Gueron and Liron, 1992
μ	0.001 kg/(m · s)	The viscosity of water (at 20°C) (Gueron and Liron, 1992)

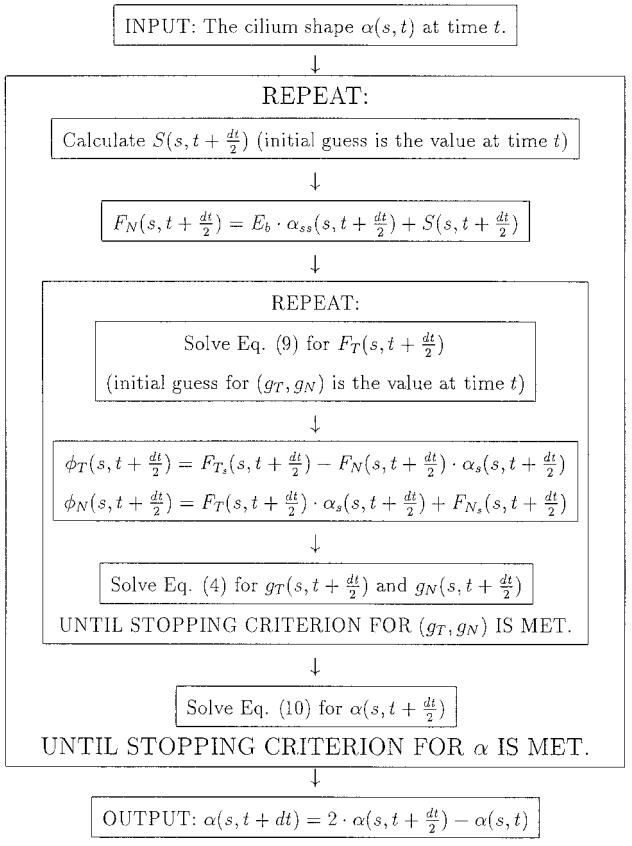

FIGURE 1 A schematic representation of the simulation algorithm.

niques used in the simulations and the complete details schematically outlined in the Appendix.

Boundary and initial conditions

Here we use boundary conditions appropriate for cilia that are stiff at the base (Blum and Hines, 1979; Murase, 1992), namely

$$\alpha_s(0, t) = 0. \tag{12}$$

We assume here vanishing drag force at $s = 0$ as an approximation motivated by the small amplitude motion near $s = 0$:

$$F_{T_s}(0, t) = F_{N_s}(0, t) = 0. \tag{13}$$

Using Eq. 11 at $s = 0$ and Eq. 13, we obtain

$$\alpha_{sss}(0, t) = -\frac{S_0 L^2}{E_b} S_s(0, t). \tag{14}$$

Forces and moments vanish at $s = 1$, and hence

$$F_N(1, t) = F_T(1, t) = 0, \tag{15}$$

which yields

$$\alpha_{ss}(1, t) = -\frac{S_0 L^2}{E_b} S(1, t). \tag{16}$$

To complete the choice of the boundary conditions we choose

$$\alpha_s(1, t) = 0, \tag{17}$$

which implies that the distal end of the cilium is straight. We use the initial conditions

$$\alpha(s, 0) = \frac{\pi}{2}, \tag{18}$$

implying that the cilium stands erect at time $t = 0$.

RECONSTRUCTION OF THE ACTIVE SHEAR FORCE FROM DATA

In this section we describe a general framework for computing and modeling the active shear force (engine) generated by the internal mechanism of the cilia and demonstrate its implementation with specific data. We separate the beat cycle into four distinct phases that occur in the following order. Phase 1: The effective stroke where the cilium beats approximately as a straight rod. Phase 2: A geometrically controlled switch from the effective to the recovery stroke, initiating a change in the direction of the motion and a bend at the basal end. Phase 3: The recovery stroke where the bend propagates along the cilium until it becomes straight again. Phase 4: A second geometrically controlled switch from the recovery to the effective stroke, initiating a new effective stroke.

We thus construct two different simple models for the forward (effective) and backward (recovery) motions, where the transitions from one to the other occur due to switches (see Satir, 1985) activated by the momentary geometric configuration of the cilium. The rationale for using two different models is that observations show completely

different behavior during the effective and recovery strokes, and there is some evidence that these phases are related to different connections among the nine filaments (Sleigh and Barlow, 1982; Satir, 1985). Configuration-dependent switches are a reasonable modeling assumption that attempt to reflect the load dependence of the internal engine. These are motivated by the fact that observed beat frequencies change in response to external load.

The exact details of the motion of a single cilium are difficult to separate since experiments always describe the motion of an ensemble of cilia. Therefore, it is difficult to determine whether the modeling principles we propose here, or their implementation, apply in general. In the present study we consider cilia that beat in a two-dimensional pattern for which both the effective and the recovery strokes occur at a plane perpendicular to the surface from which the cilia emerge. For data we use the cilium of *Paramecium*, whose beat pattern is close to being two-dimensional (Sleigh, 1962). We use these observed beat patterns to compute locations and velocities at various times during the beat cycle. Then we calculate the forces that are responsible for the observed motion and fit to a simple functional form that represents the model engine. We do not attempt to account here for the specific details of how these forces are generated and controlled by internal structure of the cilium. Nevertheless, it is known that the internal shear forces arise from the dynein cross-bridges and from the radial spokes and nexin links systems (Sleigh and Barlow, 1982). It is thus convenient to follow Hines and Blum (1978) and to consider these two systems separately, and to write

$$S(s, t) = S_d(s, t) + S_r(s, t), \tag{19}$$

where S_d and S_r represent the shear forces due to the dynein cross-bridges and to the radial spokes/nexin links systems, respectively.

The implementation of our proposed modeling approach to a specific case is based on the available data on the observed beats. While the forces that generate the motion are quite accurately reconstructed, there are more than one option to model their control, in particular how the model engine responds to external load. Our modeling assumption is that the load dependence is reflected only through the geometric switches; that is, the internal mechanism does not change its properties due to load. A different approach that would produce a different, perhaps even more realistic model of the internal ciliary mechanism would be to include the property that dyneins generate more forces when slowed down by load. This would actually replace our configuration-dependent engine with a speed-dependent one. Without actual quantitative data, this approach must involve another modeling assumption. One example is Brokaw (1985) who included this property without going into details of the internal structure. His approach can also be explored within our modeling framework.

The effective stroke

During the effective stroke the cilium moves approximately as a straight rod. If the angular velocity is denoted by ω_{eff}, the tangential and the normal components of the velocity are

$$V_T = 0, \quad V_N = -\omega_{eff} s, \tag{20}$$

and the drag-velocity equations (Eq. 2) reduce to:

$$\phi_N = \bar{C}_N \omega_{eff} s + g_N, \tag{21}$$

$$\phi_T = g_T. \tag{22}$$

Substituting Eq. 21 into Eq. 6, and using $\alpha_s = 0$, yields

$$F_{N_s} = \bar{C}_N \omega_{eff} s + g_N. \tag{23}$$

The distal end of the cilium is free, and thus the shear forces vanish at $s = 1$. We integrate Eq. 23 with respect to s and obtain

$$F_N(s, t) = \bar{C}_N \omega_{eff} \frac{(s^2 - 1)}{2} + f(s, \alpha(t)), \tag{24}$$

where

$$f(s, \alpha(t)) = -\int_s^1 g_N(\xi, t) d\xi. \tag{25}$$

Since the cilium is straight, the elastic forces vanish and Eq. 11 gives:

$$\begin{aligned} S(s, t) &= F_N(s, t) \\ &= \bar{C}_N \omega_{eff} \cdot \frac{(s^2 - 1)}{2} + f(s, \alpha(t)). \end{aligned} \tag{26}$$

To compute the active shear force, $S(s, t)$, we solve the integral equations (Eq. 2) for ϕ_N and ϕ_T, and then solve Eq. 6 for F_N and F_T.

Fig. 2 *a* displays the calculated active shear force, S, for different positions during the effective stroke, and panel *b* displays $f[s, \alpha(t)]$, which is calculated at these inclination angles. As shown in panel *b* the computed function $f[s, \alpha(t)]$ behaves roughly like $C \cdot [(s^2 - 1)/2]$, with an angle-dependent constant $C = C[\alpha(t)]$. Note that if we use the G-H approximation instead of the more accurate GL hydrodynamics, the active shear force turns out to be angle-independent, which gives a less realistic description of the engine. We model the function $f[s, \alpha(t)]$ by

$$f(s, \alpha(t)) = \bar{C}_N \omega_{eff} \cdot h(\alpha(t)) \cdot \frac{(s^2 - 1)}{2}, \tag{27}$$

where $h(\alpha)$ represents the angle dependence. From the expression for g_N it follows that $f(s, \alpha)$ is symmetric about

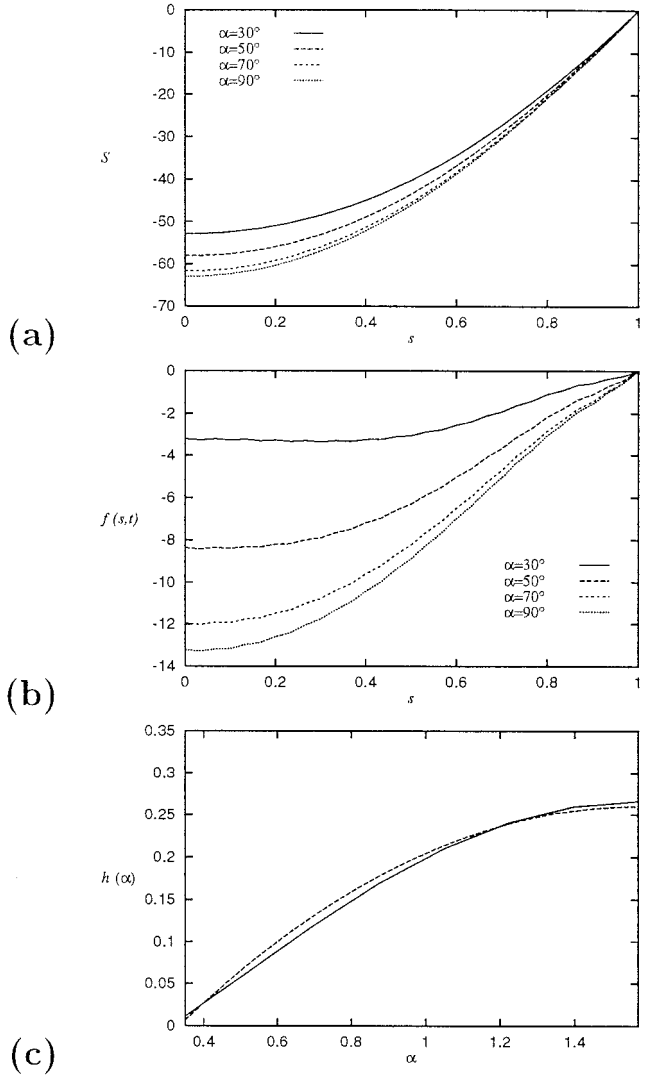

FIGURE 2 (*a*) The computed active shear force S during the effective stroke, for different values of the inclination angle α. (*b*) The function $f[s, \alpha(t)] = -\int_s^1 g_N(\xi, t)d\xi$ computed during the effective stroke for the same values of α as in (*a*) (see explanation in the text). (*c*) $h(\alpha)$ as a function of α during the effective stroke. The solid line represents calculation results, the dashed line is the fitted curve $h(\alpha) = A_1 + A_2 \cdot (\alpha - \pi/2)^2$ (with $A_1 = 0.26$ and $A_2 = -0.17$). The units of the horizontal and the vertical axes in (*a*) and (*b*) are nondimensional length and nondimensional force, respectively. The horizontal axis in (*c*) measures the inclination angle α in radians.

$\alpha = \pi/2$, and we thus fit $h(\alpha)$ by

$$h(\alpha) = A_1 + A_2 \cdot \left(\alpha - \frac{\pi}{2}\right)^2. \quad (28)$$

Fig. 2 *c* shows the graph of $h(\alpha)$ versus α, as obtained from these calculations, and the fitted function defined by Eq. 28. A_1 and A_2 are computed by a minimum least-squares fit, which yields $A_1 = 0.26$ and $A_2 = -0.17$. Evidently, this simple procedure produces a relatively good fit.

Finally, the shear force during the effective stroke is modeled by

$$S = \bar{C}_N \omega_{eff} \cdot \frac{(s^2 - 1)}{2} \cdot \left[1 + A_1 + A_2 \cdot \left(\alpha - \frac{\pi}{2}\right)^2\right]. \quad (29)$$

Note that $\bar{C}_N$ and ω_{eff} appear only as the combination $\bar{C}_N \omega_{eff}$. We use the two parameters separately in order to leave a frequency term (ω_{eff}) and for consistency with the GL equations. The values we use for ω_{eff} and $\bar{C}_N$ are based on the data, as detailed in the next section.

According to Sleigh and Barlow (1982) the radial spokes are attached to the central complex along the bent region but are not connected along the straight regions. Since during the effective stroke the cilium is almost straight, the contribution from the radial spokes system ($S_{r_{eff}}$) may be ignored. Thus, active shear force during the effective stroke (S_{eff}) is modeled by

$$S_{eff} = S_{d_{eff}} + S_{r_{eff}} = \bar{C}_N \omega_{eff} \cdot \frac{(s^2 - 1)}{2} \cdot [1 + h(\alpha)]. \quad (30)$$

The recovery stroke

Data handling for computing the velocities during the recovery stroke

Calculation of the active shear force during the recovery stroke is more complicated than during the effective stroke because the angular velocity of the cilium varies with s. To determine the velocities during the recovery stroke, we use the beat cycle diagrams shown by Sleigh (1962, 1968) as data. We fix N points, equally spaced by $ds = 1/N$ arclength apart, along the cilium at all positions during the observed recovery stroke, and measure $x = x(s, t)$ and $y = y(s, t)$ at these grid points. The number of positions, separated by fixed time intervals dt, is $K + 1$. We end up with $K + 1$ sets of coordinates $[x(ids, jdt), y(ids, jdt)] = (x_i^{(j)}, y_i^{(j)})$, $0 \le i \le N$, $0 \le j \le K$. To suppress measurement errors we smooth the manually measured data and fit $\alpha(s)$ by the sigmoidal function $A/[1 + \exp(B \cdot s - C)] + D$ as shown in Fig. 3 *b*. The reconstructed recovery stroke is displayed in Fig. 3 *a*. Finally, the (x, y)-components of the velocity at these points are approximated by a central difference.

Blake (1972) and Liron and Mochon (1976) tackled a similar reconstruction problem. They used Fourier time series for describing the coordinates of the moving cilium, computing the coefficients from the observed data. Since our typical data represent a relatively small number of positions during the beat, only a few terms can be included in such Fourier series, and then the related derivatives would not approximate the cilium's velocity well. We therefore prefer the central difference approximation, described above.

Calculation of the active shear force

Using the fitted velocity we solve the integral equations (Eq. 2) for the drag forces ϕ_T and ϕ_N. Equation 6 are then solved

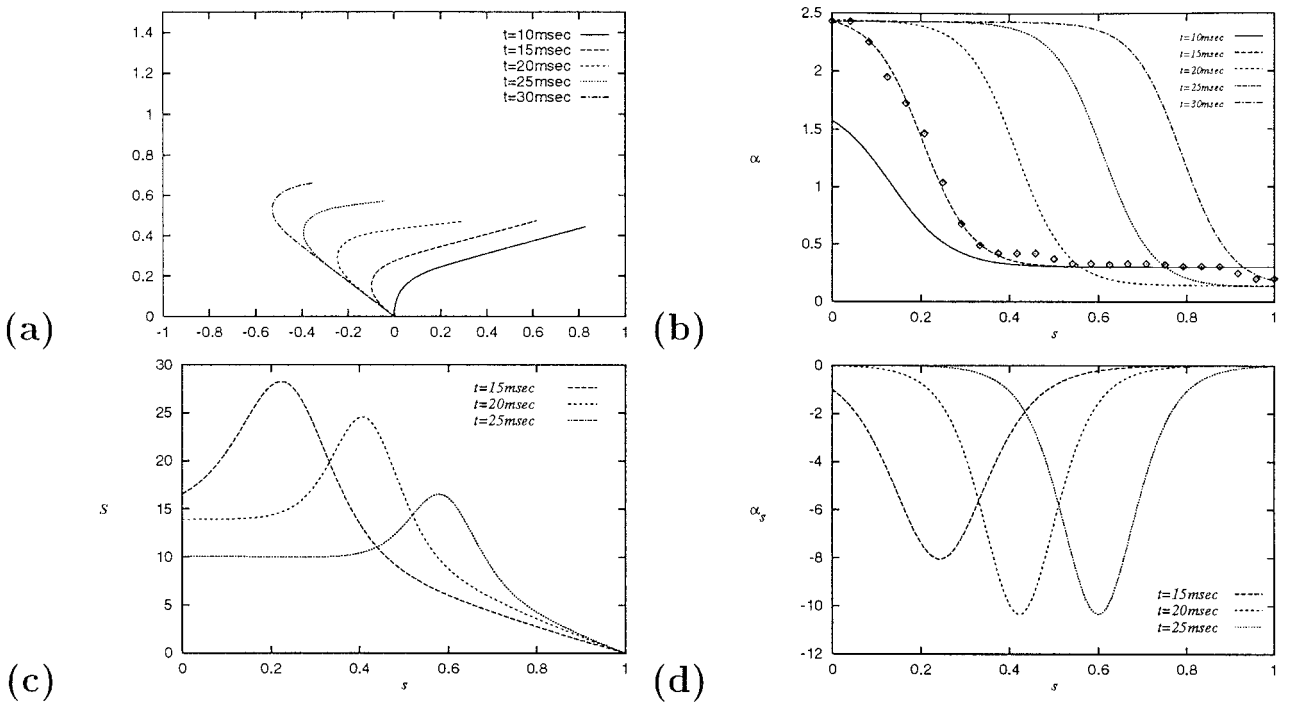

FIGURE 3 (*a*) Five positions during the recovery stroke, reconstructed from the diagrams of the beat cycle of *Paramecium* [Sleigh (1962); (see explanation in the text)]. (*b*) The curvature α as function of s at the five positions during the recovery stroke. The diamond symbols shown with one of the curves display the measured values for corresponding time step. The curves are results of smoothing by sigmoidal functions (see explanation in the text). (*c*) The calculated shear force along the cilium at three times during the recovery stroke. (*d*) α_s as function of s during the recovery stroke at the same time positions as in (*c*). The units of the horizontal axis in (*a*)–(*d*) are nondimensional length. The units of the vertical axis are (*a*) nondimensional length; in (*b*) radians; (*c*) nondimensional force; (*d*) dimensionless curvature.

for F_N and F_T, and the active shear force generated inside the cilium (S) is obtained from Eq. 11.

Fig. 3 *c* displays the calculated shear force as a function of s at different time steps during the recovery stroke. These are the same time steps as in panel *d*, where the curvature of the cilium is plotted. The peak observed in these curves can be interpreted by the following argument: when the bend is at $s = s_b$, the region $0 \le s \le s_b$ has already reached its leftmost, almost straight, position (see Fig. 3 *a*). Therefore, the force required to maintain it fixed is approximately constant. A stronger force is required to overcome the elastic bending resistance near the region $s \sim s_b$ and to propagate the bend toward the distal end of the cilium.

Recall that we construct the engine as the sum of the forces due to the dynein cross-bridges and to the radial spokes/nexins (see Eq. 19). A reasonable and straightforward indicator of the location of the bend is the curvature of the cilium. Indeed, the peak of the active shear force obtained by our calculations is located at the place of maximal curvature of the cilium (compare panels *c* and *d* of Fig. 3). Thus, we model the contribution of the radial spokes to the active shear force ($S_{r_{rec}}$) by a simple function of the curvature, namely

$$S_{r_{rec}}(s, t) = B_{rec} \cdot \alpha_s(s, t), \tag{31}$$

where B_{rec} is a parameter to be computed by fit to the data.

Similarly to the effective stroke case, we model the forces due to the dynein cross-bridges ($S_{d_{rec}}$) by a parabolic function:

$$S_{d_{rec}}(s, t) = \bar{C}_N \omega_{rec} \cdot \frac{(1 - s^2)}{2} \cdot [1 + h_{rec}(\alpha)], \tag{32}$$

where ω_{rec} is the typical velocity of the recovery stroke (e.g., the velocity of bend propagation along the cilium) and $h_{rec}(\alpha)$ is a function of the form (Eq. 28). Sleigh and Barlow (1982) reported that the dynein cross-bridges work synchronously along the cilium during the effective stroke. They assumed that at the beginning of the recovery stroke the dynein arms work only at the basal region, thus initiating the bend. We adopt this assumption and model the dynein arms activity by using the following form for $h_{rec}(s, t)$:

$$h_{rec}(s, t) = \begin{cases} 1 + A_1 + A_2 \cdot \left(\alpha(0, t) - \dfrac{\pi}{2}\right)^2, \\ \quad 0 \le s \le 0.1 \quad \text{and} \quad \alpha(0, t) < \alpha_L \\ A_1 + A_2 \cdot \left(\alpha(0, t) - \dfrac{\pi}{2}\right)^2, \\ \quad 0.1 < s \le 1 \quad \text{or} \quad \alpha(0, t) > \alpha_L \end{cases} \tag{33}$$

Here, α_L is the inclination angle of the cilium at its leftmost position, just before the beginning of the effective stroke. The values of A_1 and A_2 are determined by fit to data.

Summary of the engine equations

We now assemble Eqs. 28, 30, 31, 32, and 33, and use the fact that the curvature vanishes during the effective stroke, which implies that no forces arise from the radial spokes system ($S_{r_{eff}} = 0$), to write the resulting expression for the active shear force:

$$S_{\text{eff/rec}} = S(s,t) = (\pm 1)\cdot\left\{\bar{C}_N \omega_{\text{eff/rec}}\cdot\frac{(s^2-1)}{2}\cdot[1+h_{\text{eff/rec}}(s,t)] + B_{\text{eff/rec}}\cdot\kappa(s,t)\right\}, \quad (34)$$

where the functions $h_{\text{eff}}(s,t)$ and $h_{\text{rec}}(s,t)$ are described by Eqs. 28 and 33 for the effective and recovery strokes, respectively. $\omega_{\text{eff/rec}}$ are the typical velocities during the effective and recovery strokes, respectively. $B_{\text{eff/rec}}$ is a parameter controlling the relative magnitude of the contribution of the radial spokes to the active shear force during the effective and recovery strokes. The sign of $S(s,t)$ is taken positive during the effective stroke and negative during the recovery stroke.

Altogether five parameters control the effective stroke [ω_{eff}, α_R, B_{eff}, and set (A_1, A_2)] and five parameters [ω_{rec}, α_L, B_{rec}, and set (A_1, A_2)] control the recovery stroke. ω_{eff}, ω_{rec}, α_R, and α_L are measured directly from the data and B_{eff}, B_{rec}, and the two sets (A_1, A_2) are obtained by fit to this data. The choice of parameters is detailed in the next section.

Switching

To complete the description of the engine it is necessary to determine when the switching between the two phases of the beat occurs. If $\sigma(s)$ denotes the effective shear (i.e., the effective amount of sliding), then the inextensibility of the filaments implies

$$\alpha(s) = \sigma(s) + [\alpha(0) - \sigma(0)] \quad (35)$$

[note that the effective shear is a geometric quantity, not to be confused with the active shear force. For details see Hines and Blum (1978)]. In our model we assume that switching occurs when further sliding is no longer possible, and then sliding in the opposite direction begins. Thus, the maximal effective displacement (σ) is achieved at the switching moment. This leftmost (or rightmost) position, corresponds, according to Eq. 35, to an inclination angle denoted α_L (α_R). Consequently, switching between the effective and the recovery strokes occurs when the cilium reaches its rightmost inclination. During the recovery stroke the cilium straightens until it reaches its leftmost early straight position. In our model, switching between the recovery and the effective strokes occurs when $\|\kappa\|_\infty < \epsilon$ (we used $\epsilon = 10^{-4}$).

NUMERICAL METHODS AND THE CHOICE OF PARAMETERS

The parameters we use in the model are listed in Table 1. With these parameter values the modified resistance coefficients for cilia beating in water are:

$$C_T = 0.0025175\,\frac{\text{kg}}{\text{m}\cdot\text{s}}, \quad C_N = 0.0035947\,\frac{\text{kg}}{\text{m}\cdot\text{s}}.$$

Note that the values of these coefficients are different from the values used with the G-H model. Particularly, the ratio C_N/C_T is 1.43, which is much lower than the value of 2 used in the G-H model and also lower than the value of 1.8 measured (roughly) for a flagellum by Brokaw (1972).

For modeling the active shear force function we use the following nondimensional parameters:

$\omega_{\text{eff}} = 393$ the average angular velocity of the cilium of *Paramecium* during the effective stroke (expressed in nondimensional units, and equivalent to 11000 °/s). Sleigh (1962).

$\omega_{\text{rec}} = 82$ the average velocity of bend propagation during the recovery stroke (expressed in nondimensional units, and equivalent to 2292 °/s). Sleigh (1962).

The parameters defining the functions $h(\alpha)$ as in Eqs. 28 and 33 are fit to the data:

	A_1	A_2
during the effective stroke	0.26	− 0.17
during the recovery stroke	1	− 2

The parameters $B_{\text{eff/rec}}$ (see Eq. 34) are:

$$B_{\text{eff}} = 0, \quad B_{\text{rec}} = 2.$$

We used finite difference schemes and iterative techniques to solve the differential and integral equations. The time step for the numerical schemes was $dt = 0.1$ ms (0.28 in nondimensional time). The nondimensional spatial step is $ds = 1/30$ (i.e., 31 discretization points on each cilium). We verified that the results do not change significantly if the number of the discretization points is increased or if the time step is decreased.

To facilitate the reproduction of our method, the details of all the computational procedures used in the numerical calculations are outlined in the Appendix.

RESULTS

Results for a single cilium

Fig. 4 *a* displays the beat cycle of a model cilium with the engine described by Eq. 34 and the parameter values described in the previous section. The beat duration (translated back to dimensional units) is ≈34 ms, corresponding to a beat frequency $w \approx 29$ Hz. For comparison, the beat duration and frequency of the cilia of *Paramecium* which we

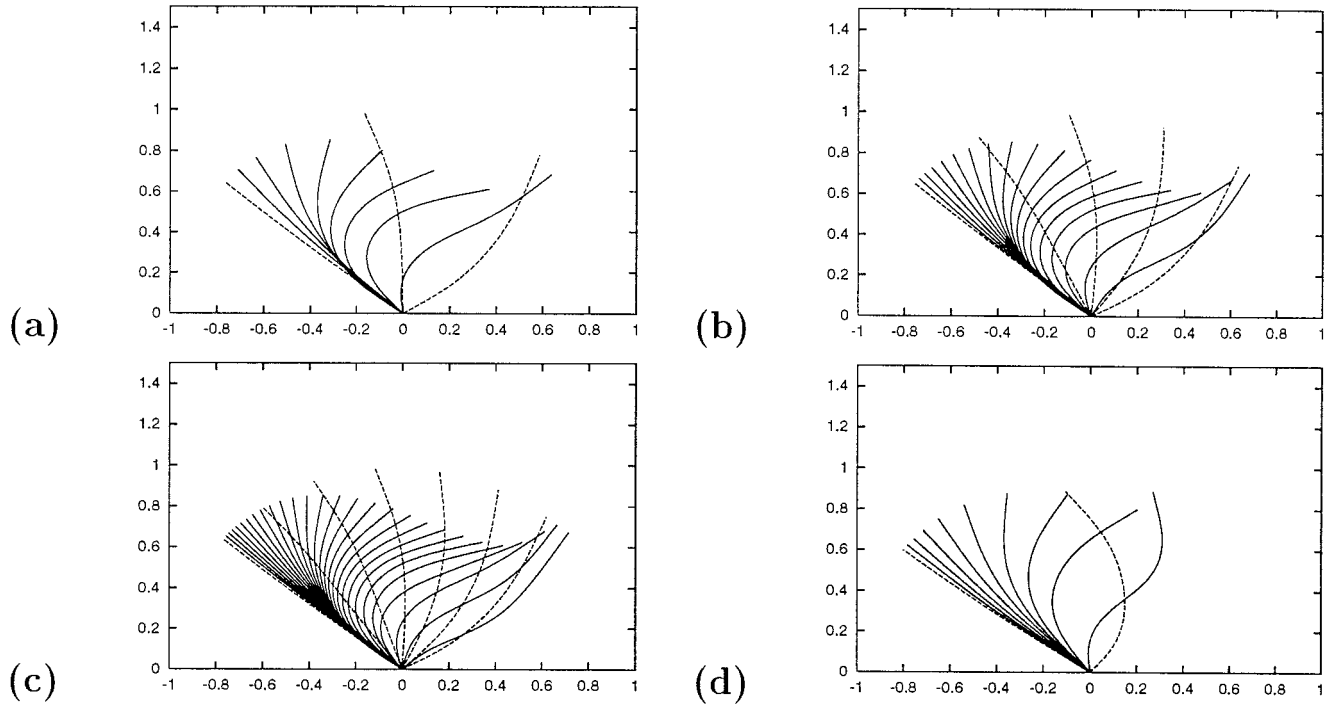

FIGURE 4 Beat cycles of model cilia. All positions are equally separated in time by 3 ms. The effective stroke positions are plotted by dashed lines and the recovery stroke positions by solid lines. The units of the axes are nondimensional length. (*a*) A single cilium. The viscosity of the surrounding fluid is that of water ($\mu = \mu_{water}$). The resulting beat frequency is ≈29 Hz. (*b*) $\mu = 2\mu_{water}$. The resulting beat frequency is ≈15 Hz and the beat pattern is changed. (*c*) $\mu = 3\mu_{water}$. The resulting beat frequency is ≈10 Hz and the beat pattern is further changed. (*d*) Side view of an infinite line of synchronized cilia, spaced by 0.3 ciliary length, beating in water. The resulting beat frequency is ≈29 Hz. Note the different angular spread during the beat as compared to the single cilium in (*a*).

used as data for the modeling process, are 35 ms and w = 28 Hz, respectively (see Sleigh, 1962, 1968). The duration of the effective and the recovery strokes of the model cilium are ≈8–9 ms and ≈25–26 ms, respectively. The duration of the effective stroke is approximately one-third of the duration of the recovery stroke for both the real and the model cilium.

During the recovery stroke, the basal region (~10% of the cilium) moves quickly from its rightmost position (the position of the beginning of the recovery stroke) to its leftmost position (the position of the beginning of the effective stroke) and remains there until the cilium straightens (see Sleigh, 1962, 1968). This also happens with the model cilium. Note also that a realistic forward bend in the cilium is formed during the effective stroke, although originally the cilium was considered as a straight rod during this phase. The autonomous formation of this bend is due to the fit approximation used when modeling S (and additionally because after a few cycles, the cilium does not start its effective stroke from a perfectly straight position). We point out that if the boundary condition $\alpha_s(0, t) = 0$ (for a cilium stiff at the base) is replaced with $\alpha(0, t) = \pi/2$ (for constantly erect cilium at the anchor), the bend formed during the effective stroke is in the opposite direction, unlike observed beats. The duration of the swing of the basal region during the recovery stroke is ≈8 ms, and the basal region remains at its leftmost position for ~75% of the beat cycle. The angular range of the effective stroke is ≈110°–115° for both the real and the model cilium. These features of the model beat cycle fit the data very well, although the actual beat pattern of the model cilium (Fig. 4 *a*) is a bit different from that of the observed cilium (Fig. 3 *a*). This difference is probably the result of the fit approximations, numerical and measurement errors, and the uncertainty of what happens at the beginning of recovery stroke. In addition, the observed cilium presented by Sleigh (1962) is one cilium within a multicilia configuration, and therefore the interaction between an unknown number of neighboring cilia is already included in the data. Nevertheless, the model beat cycle possesses the typical features of the beat. Table 2 compares some properties of the cilium of *Paramecium* with those obtained from the model, demonstrating a good fit to the data.

The effects of increased viscosity

Machemer (1972) investigated the effects of increased viscosity on the cilia of *Paramecium*, particularly the effects on the beat frequency. He reported that beat frequency decreases exponentially with increasing viscosity.

Fig. 4, *a–c* displays the beat patterns of the model cilium at three different viscosities. With increased external load

TABLE 2 Comparison between the properties of model beats and observed ciliary beats of *Paramecium*

Parameter	Dimensions	Data (Sleigh, 1962)	Model
Beat duration	ms	35.7	≈34
Beat frequency	cycles/s	28	≈29.5
Angular range of the effective stroke	degrees	110	110–115
Duration of the effective stroke	ms	≈9	≈8
Duration of the recovery stroke	ms	≈26	≈26
Ratio of durations (recovery/effective)		2.9	3.25
Duration of the basal swing during the recovery stroke	ms	6	≈7

the cilium changes its beat pattern; the bend at the beginning of the recovery stroke becomes deeper and the beat duration lengthens. However, the ratio between the durations of the effective and the recovery strokes changes only slightly (roughly 1:3). This reflects the fact that our model engine does not change with increased load. We conclude that during the effective stroke the engine is strong enough to overcome viscous resistance in this range, but with increased external load it becomes more difficult to propagate the bend along the cilium. Fig. 5 compares the dependence of the beat frequency on viscosity of the model cilium with Machemer's data (Machemer, 1972). The model beat frequency decreases roughly linearly when plotted against the logarithm of the viscosity in the region $\mu_{water} \leq \mu \leq 5\ \mu_{water}$, as reported by Machemer. This feature was *not* explicitly assumed in the model and thus demonstrates that our model captures this important property of the ciliary

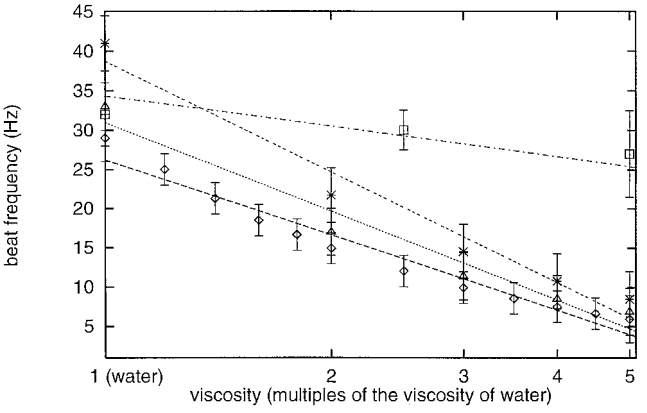

FIGURE 5 Dependence of beat frequency on viscosity in the range $\mu_{water} \leq \mu \leq 5\mu_{water}$. Diamonds (◇), triangles (△), and asterisks (∗) are the modeling results for a single cilium and for five adjacent cilia separated by 0.6 and 0.3 ciliary length, respectively, with the errors indicated as vertical bars. The lines (— —, · · · · ·, and – – –) are the least-squares linear fit to the computed values. The uppermost line (— · — · —) shows the fit (in the range $\mu_{water} \leq \mu \leq 5\mu_{water}$) to the experimental results (□) obtained for *Paramecium* by Machemer (1972). The abscissa is on a logarithmic scale.

motion. We also mention that the case of an isolated cilium we discuss here is a hypothetical one. In reality there are always neighboring cilia, and the beat frequency is also affected by the external flow that is induced by the neighboring cilia. Machemer's observations were made with a real multicilia configuration (not specified). This can explain the difference between the slope of the model results and the real data. However, note that the beat frequency of the model cilia tends to approach that of the real data as we simulate a row of several adjacent cilia.

Machemer investigated the behavior of cilia when the fluid viscosity was increased by as much as 40 times that of water. He found that with increased viscosity (above 5 μ_{water}) *Paramecium* changes the plane of beating. Since our model does not include this possibility, we examined the effects of increased viscosity only in the range [μ_{water}, 5 μ_{water}].

We also examined the effects of changed viscosity on the beat frequency of an infinite line of cilia spaced parallel to one another (see below for details). The dependence of the beat frequency turned out to be similar to that for an isolated cilium (see Table 3), but at each viscosity the beat frequency of the cilia in the infinite line of cilia was somewhat higher than the frequency of a single cilium at that viscosity.

The effect of external flows

To further examine the load dependence of the model engine we studied the influence of external flow on the resulting beat frequency. We used a parallel flow satisfying no-slip conditions on the surface, and with linearly growing amplitude: $(V_x, V_y) = (K_0 \cdot y, 0)$, where K_0 is a constant (possibly time-dependent). Nondimensional flow of magnitude K_0 corresponds to $3.36 \cdot 10^{-4} \cdot K_0$ m/s with the present choice of parameters. Three different cases were tested: 1) flow in the direction of the effective stroke; 2) flow in the direction of the recovery stroke; 3) periodic flow.

Fig. 6, *a–c* displays the ciliary beat cycles when the external flow is in the direction of the effective stroke. Increasing K_0 shortens the effective stroke and the whole beat pattern (stopping positions, angular range, duration of the effective and recovery strokes) changes. During the recovery stroke the cilium experiences stronger resistance due to the external flow, and the resulting recovery stroke takes longer. As the flow in this direction becomes stronger,

TABLE 3 The combined effect of cilia interactions and increased viscosity

Viscosity	Single Cilium	Two Cilia Configuration	Five Cilia Configuration	One Infinite Line
μ_{water}	29 Hz	31 Hz	33 Hz	32 Hz
$2\mu_{water}$	17 Hz	19 Hz	20 Hz	20 Hz
$3\mu_{water}$	12 Hz	13 Hz	13 Hz	14 Hz

Comparison of the beat frequency for three different values of viscosity and for four configurations. The spacing between adjacent cilia is 0.6 in all multicilia configurations.

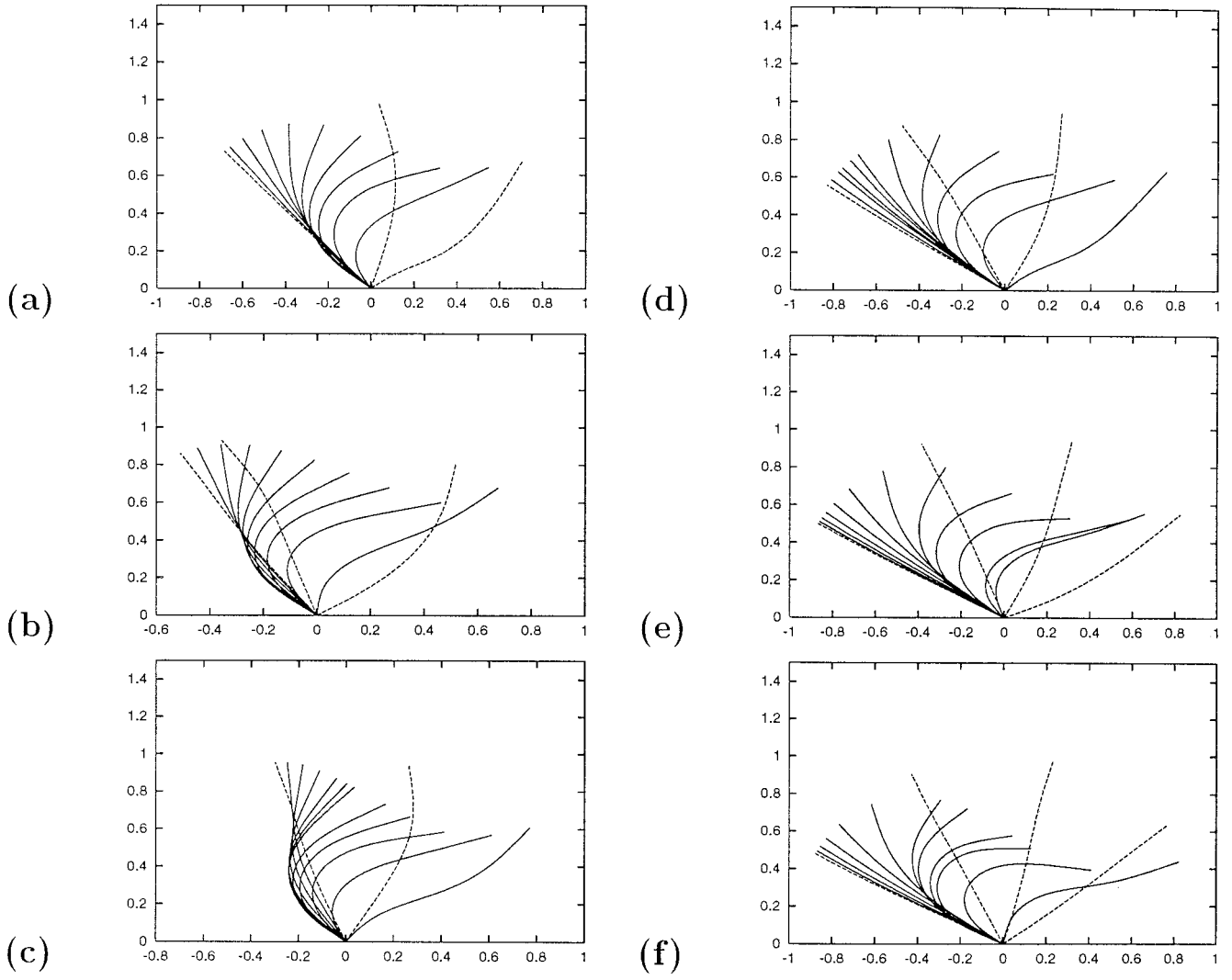

FIGURE 6 Beat cycles of a single cilium showing the effects of external flows. All positions are equally separated in time by 3 ms. (*a*)–(*c*) the external flow is in the direction of the effective stroke. $(V_x, V_y) = (K_0 \cdot y, 0)$, where $K_0 = 1, 2, 3$, respectively. (*d*)–(*f*) the external flow is in the direction of the recovery stroke. $(V_x, V_y) = (K_0 \cdot y, 0)$, where $K_0 = -1, -2, -3$, respectively. The units of the horizontal and vertical axes are nondimensional cilium length. Beat patterns, angular spread, and beat frequency change due to the external flow.

one can see that the resistance changes the final position at the end of the recovery stroke.

Fig. 6 *d–f* displays the ciliary beat cycles when the external flow is in the direction of the recovery stroke. Such flow poses more resistance to the cilium during its effective stroke. The duration of the effective stroke lengthens with increased flow amplitude, and the beat pattern changes. Table 4 summarizes some of the results obtained with these flows.

The periodic external flow tested was $(V_x, V_y) = [K_0 \sin(2\pi wt)y, 0]$ in the range $0.5w_0 \leq w \leq 2w_0$ (that is from half the frequency of a beating cilium to twice that frequency), and for $1 \leq K_0 \leq 15$. We found that the beat frequency of the model cilium approximates the frequency of the external flow. This is consistent with the experimental evidence reported by Okuno and Hiramoto (1976), who reported that starfish sperm flagella synchronize their beat frequency to that of a nearby vibrating microneedle, and also with the results of similar experiments by Eshel and Gibbons (1989) on sea urchin sperm flagella.

TABLE 4 The effect of external flow on beat frequency

Velocity (V_x, V_y)*	Beat Duration (ms)	Beat Frequency (beats/s)	Eff. Stroke Duration (ms)
$(1 \cdot y, 0)$	34.5	29	6
$(2 \cdot y, 0)$	35.5	28	5.5
$(3 \cdot y, 0)$	38	26	4
$(-1 \cdot y, 0)$	37	27	8
$(-2 \cdot y, 0)$	42	24	9
$(-3 \cdot y, 0)$	40	25	11

*Positive and negative V_x components represent flows in the direction of the effective and the recovery strokes, respectively.

Two-cilia configuration

Our model results indicate that when two cilia are spaced by more than two cilia lengths, their influence on each other becomes negligible. Fig. 7 shows (on a logarithmic scale) the ratio of the beat frequency of a two-cilia configuration to that of a single cilium as a function of the distance between the two cilia. We see that cilia that beat close to each other tend to beat faster. For example, if the distance between the cilia decreases from 2 to 0.3, the beat frequency rises from ≈29 Hz (the beat frequency of a single cilium) to ≈40 Hz. The dashed line in Fig. 7 is the least-squares fit to the function $A \cdot x^B$, and the extrapolation of this fitted line back to the distance 0.02 predicts a beat frequency of ≈53 Hz. Since the radius of our model cilia is $a = 0.01$ (see Table 1) this distance represents two touching cilia. To test the prediction, we modeled a (very) roughly equivalent isolated cilium having the same cross-section area (i.e., with radius $\sqrt{2}a$), and beating in a fluid with viscosity 1/2 μ_{water}. The match is quite satisfactory as we found that the beat frequency of such a cilium is ≈45.5 Hz (we cannot expect a better match with such a crude approximation).

Gray (1928) reported on experiments with two flagella beating initially at different frequencies and phases. When these flagella were put close enough to each other, they tended to quickly synchronize and beat with the same frequency and in phase. Machin (1963) considered the hypothetical interaction between two adjacent flagella, each of which beating initially in a small amplitude sinusoidal pattern. Assuming that they continue to beat sinusoidally when brought into close proximity and that each one experiences a prefixed induced flow field, he obtained synchronization.

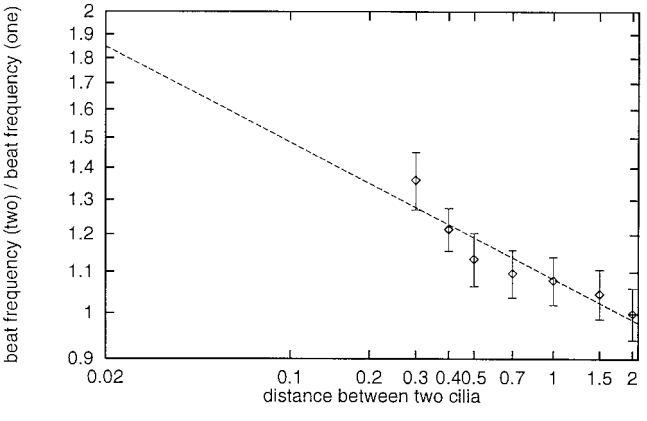

FIGURE 7 The dependence of the steady-state mutual beat frequency of two adjacent cilia, on the distance between them. The vertical axis measures the ratio of the beat frequency of two neighboring cilia to that of a single cilium after the steady state has been obtained in all cases. The horizontal axis measures the nondimensional distance between the cilia. The horizontal and the vertical axes are both on a logarithmic scale. The vertical error bars represent the estimated errors in the calculated values, and the dashed line is a least-squares fit to the function $A \cdot x^B$ with $A = 1.0829$ and $B = -0.1368$. The line is extrapolated back to the intercilia spacing of 0.02, corresponding to two touching cilia. Explanation is given in the text.

Our model, on the other hand, does not make any assumptions on the relation between the intrinsic beat pattern of the two cilia and the pattern that emerges when they are close together and subjected to the effects of their interaction. It also includes realistic interaction, and we obtain synchronization as a *dynamical* process evolving quickly and autonomously from two cilia, initially completely out of phase. A somewhat analogous phenomenon of self-synchronization and phase locking between rings and lines of coupled oscillators is well known, and was investigated experimentally and theoretically [e.g., for one-dimensional weakly coupled chains and rings of oscillators, by Ermentrout and Kopell (1984) and Ermentrout (1985)]. Here we have a complex biological system demonstrating some predictions of this theory. The evolution of self-synchronization of two model cilia that are spaced one cilium length apart and start beating completely out of phase is shown in Fig. 8. At the beginning of the simulation ($t = 0$ in the figure), the right cilium begins at its effective stroke whereas the left one begins at its recovery stroke. The two cilia synchronize within two cycles. The mutual beat frequency is ≈31 Hz, to be compared with ≈29 Hz, which is the beat frequency of a single cilium. We found similar fast self-synchronization to occur with different intercilia spacing in the range of 0.3 to 1.5 ciliary lengths.

In most realistic situations involving multicilia configurations, the cilia have identical properties, as the case stud-

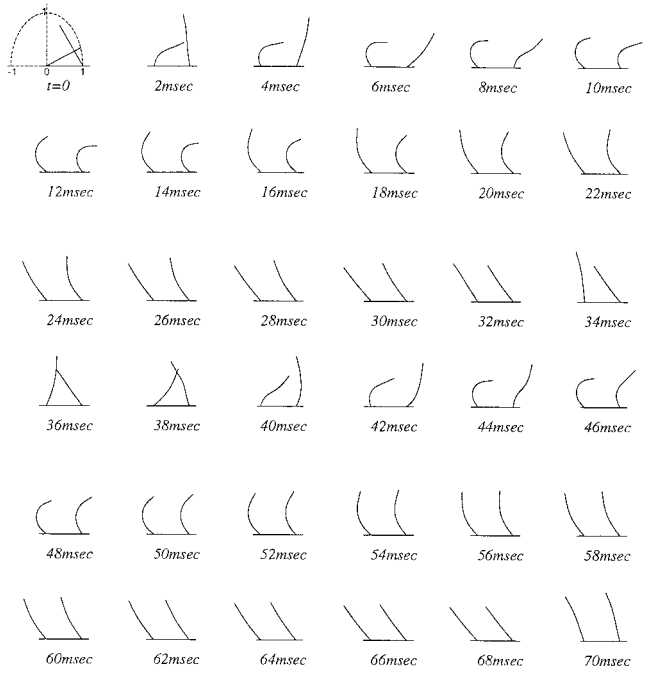

FIGURE 8 The autonomous evolution of synchronization between two identical cilia starting at $t = 0$ at opposite phases (the left cilium starts the recovery stroke and the right starts the effective stroke). Synchronization is achieved within two cycles. The resulting steady-state beat frequency is ≈31 Hz. The cilia spacing is 1, the 36 successive snapshots are separated in time by 1 ms, and the units of the axes are nondimensional length. The ellipse shown at $t = 0$ is the unit circle, appropriately distorted by different scaling along the horizontal and the vertical axes. *msec* = ms.

ied above. However, it is also interesting to investigate self-synchronization of two adjacent cilia having different engines, as shown in Figs. 9 and 10. These cilia are spaced by one cilium length apart, begin beating completely out of phase, and differ from each other in their engine parameters (ω_{eff} and ω_{rec}; one cilium has a set of parameters as described in Numerical Methods, ω_{eff} and ω_{rec} of the second cilium are doubled). If isolated and beating in water, the beat frequency of the left cilium in Fig. 9 is ≈29 Hz and that of the right cilium is ≈35 Hz. Their intrinsic beat patterns are also different. Fig. 10 shows a configuration where the positions of the cilia are switched. In both cases, the two cilia change their original beat due to the interaction and end up having two different beat patterns. Furthermore, the beats shown in Figs. 9 and 10 are also different due to the asymmetry in the positions of the cilia with respect to the direction of the effective stroke. Nevertheless, we found that in both cases the cilia match their (steady state) beat frequency at the value of ≈32 Hz, which is the average of their intrinsic beat frequencies.

The following comment, which relates to all figures that display two cilia and multicilia configurations in this paper, is important to avoid misinterpretation. Due to the intercilia separation, the relevant range along the horizontal axis is larger than the range along the vertical axis. Thus, when plotting multicilia configurations, we must use different scales for the axes. This may give the deceiving impression that the length of the cilia varies, while in fact it always remains 1 (in nondimensional units). To avoid misinterpretation of lengths in such figures, we add the image of the unit circle, centered at the anchor of the leftmost cilium. This unit circle is of course distorted into an appropriate ellipse and can be used for measuring distances on the plot.

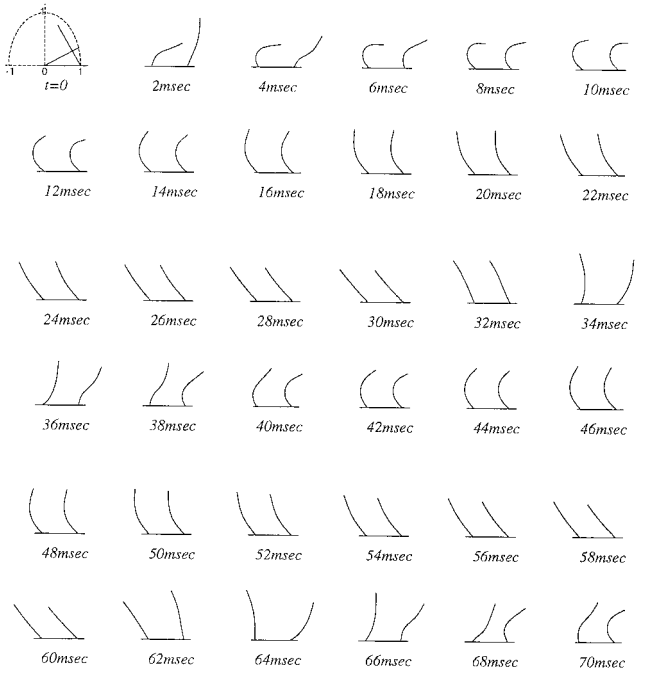

FIGURE 9 Two cilia with *different* engine parameters starting at opposite phases at $t = 0$ (the left cilium starts the recovery stroke and the right cilium starts the effective stroke). Explanation and parameters are detailed in the text. The beat frequencies of the left and the right cilium, when isolated and beating in water, are ≈29 Hz and ≈35 Hz, respectively. The beat patterns of the two cilia remain different but they synchronize their steady-state beat frequency at ≈32 Hz. The cilia spacing is 1, the 36 snapshots are separated in time by 1 ms, and the units of the axes are nondimensional length. The ellipse shown at $t = 0$ is the unit circle, appropriately distorted by different scaling along the horizontal and the vertical axes. *msec* = ms.

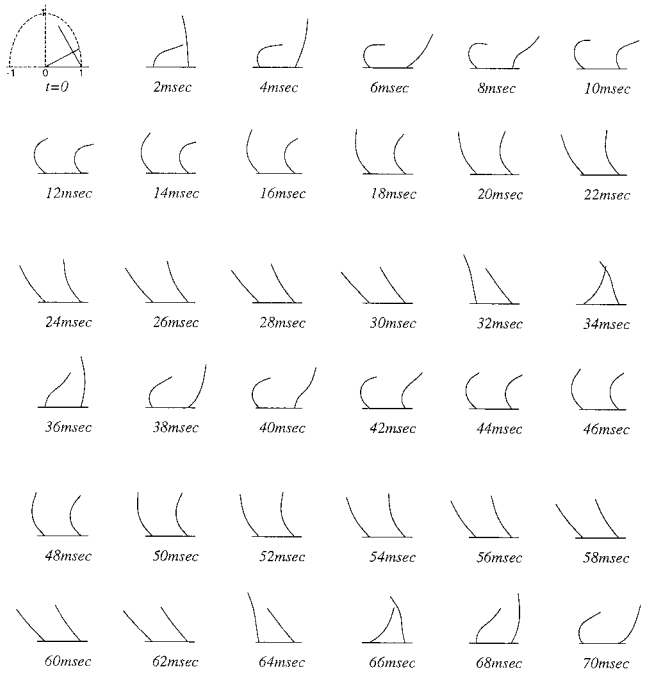

FIGURE 10 Two cilia with *different* engine parameters starting at opposite phases at $t = 0$ (the left cilium starts the recovery stroke and the right cilium starts the effective stroke). The cilia are the same as in Fig. 9, but with switched positions. The beat frequencies of the left and the right cilium, when isolated and beating in water, are ≈35 Hz and ≈29 Hz, respectively. The beat patterns of the two cilia remain different but they synchronize their steady-state beat frequency at ≈32 Hz. The cilia spacing is 1, the 36 snapshots are separated in time by 1 ms, and the units of the axes are nondimensional length. The ellipse shown at $t = 0$ is the unit circle, appropriately distorted by different scaling along the horizontal and the vertical axes. *msec* = ms.

Multicilia configurations

In nature, there may be thousands of cilia beating together, propagating a microorganism through the viscous medium, or moving fluid through a tube. One of the striking features of ciliary motion is metachronal coordination. As mentioned above it has been speculated that the metachronism phenomenon may be the result of hydrodynamical coupling. We attempt to use our model to provide some support for this conjecture.

Two-cilia and five-cilia configurations were used to study the effect of cilia interaction *and* of increased viscosity. In Table 3 we compare the beat frequencies of an isolated

cilium, of a two-cilia and a five-cilia configuration at three different viscosities. The ciliary spacing is 0.6. The table shows significant beat frequency changes in response to increased viscosity in all cases. We also used the five-cilia configuration to compare the effect of increased viscosity with the experimental data of Machemer (1972). The results are shown in Fig. 5. Note that the roughly linear dependence on the logarithm of the viscosity persists. Furthermore, the resulting line is shifted upward with respect to the line that describes a single cilium and the results tend to approach those reported by Machemer (1972). We did not repeat this experiment with larger configurations due to the prohibitive time that such simulations would take.

Figs. 11 and 12 show the beat cycles of a 10- and a 100-cilia configuration, respectively. The cilia spacing is 0.3, the successive snapshots are separated in time by 1 ms, and the 24 snapshots cover (approximately) a complete beat cycle. The displayed snapshots are taken after the cilia have already reached their steady state, and the time indicator $t = 0$ corresponds to the beginning of the fifth cycle rather than the beginning of simulations, as in the figures that show two cilia configurations. These figures demonstrate the autonomous occurrence of imperfect synchronization between the cilia. The result resembles and has many (but not all) characteristics of a metachronal wave. In both configurations the steady-state beat frequency is ≈42 Hz (beat duration 24 ms).

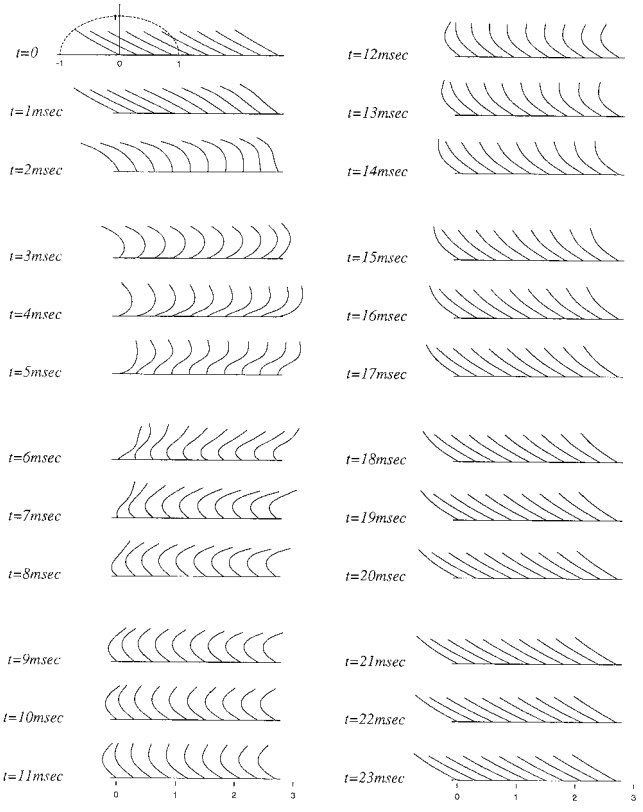

FIGURE 11 Self-organized imperfect synchronization, resembling a metachronal wave, in a row of 10 cilia. The snapshots are already at steady state: the frame $t = 0$ is the beginning of the fifth cycle of the simulation. The resulting steady-state beat frequency is ≈42 Hz, and the 24 snapshots that are separated in time by 1 ms cover a complete beat cycle. The cilia spacing is 0.3, and the units of the axes are nondimensional length. The ellipse shown at $t = 0$ is the unit circle, appropriately distorted by different scaling along the horizontal and the vertical axes. *msec* = ms.

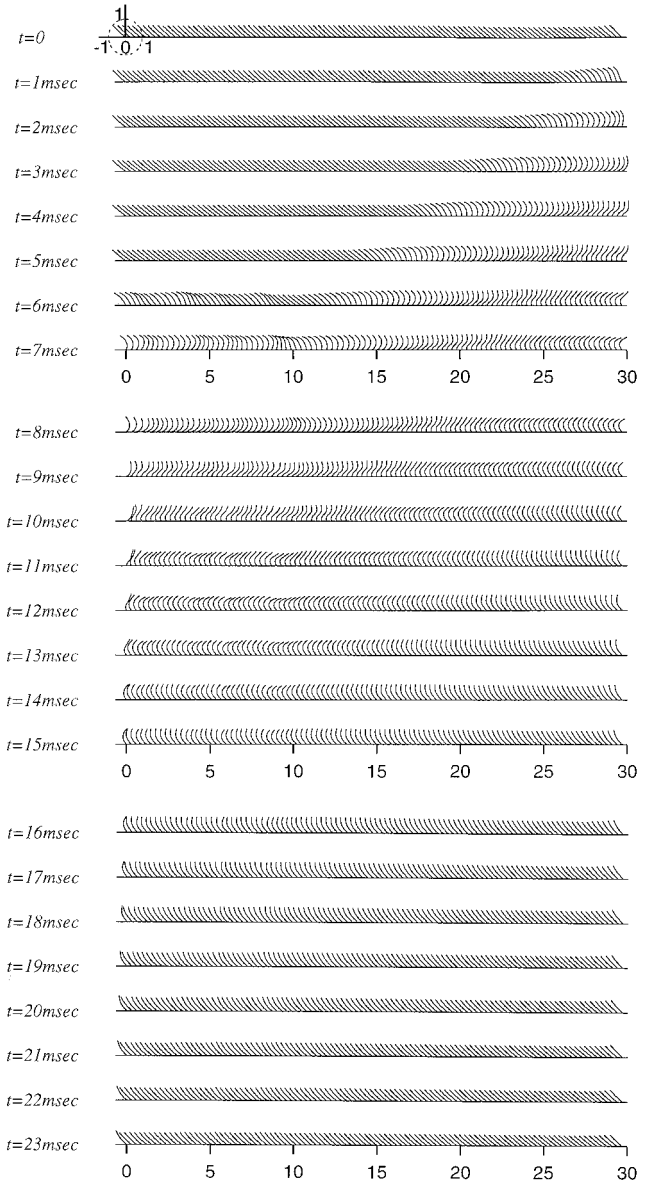

FIGURE 12 Self-organized imperfect synchronization, resembling a metachronal wave, in a row of 100 cilia. The snapshots are already at steady state: the frame $t = 0$ is the beginning of the fifth cycle of the simulation. The resulting steady-state beat frequency is ≈42 Hz, and the 24 snapshots that are separated in time by 1 ms cover a complete beat cycle. The cilia spacing is 0.3, and the units of the axes are nondimensional length. The ellipse shown at $t = 0$ is the unit circle, appropriately distorted by different scaling along the horizontal and the vertical axes. *msec* = ms.

The effective stroke in the 10-cilia configuration takes place roughly from $t = 0$ to $t = 5$ ms. To notice the phase lags between the cilia, note that at $t = 5$ ms the leftmost cilium is still at the end of its effective stroke, whereas the other nine cilia have already started their recovery stroke.

The cilia have different beat patterns, according to their position in the line.

The 100 cilia beat in an approximately antiplectic metachronal wave, propagating from right to left (the direction of the effective stroke is from left to right). This type of antiplectic metachronism may occur with the cilia of *Paramecium* under some conditions [see, for example, Machemer (1972)]. We point out that although Sleigh (1962) originally suggested that the cilia of *Paramecium* beat in an antiplectic metachronal pattern, later work showed that it was in fact dexioplectic [see Tamm (1972)]. To observe the phase lags between the cilia, note that at $t = 0$ the rightmost cilium already begins its effective stroke, whereas the other cilia are still at the end of the previous recovery stroke. Phase lags persist in the subsequent snapshots (e.g., at $t =$ 1–4 ms). A roughly wavelike pattern, formed by the tips of the cilia, propagating from the right to the left, can be seen in the snapshots (e.g., at $t = 6$ ms, $t = 9$ ms, $t = 15$ ms). Phase lags during the period of the "slow straightening back to position" of the cilia toward the end of the cycle still exist, although they are less easy to observe than during the beginning of the cycle (mainly due to the scaling in the figure).

Two-dimensional arrays of cilia beating in the same plane

In nature large numbers of cilia are arranged in almost parallel rows, such that the motion of adjacent cilia is synchronized along one direction (often perpendicular to the direction of the effective stroke), but out of phase along the other. To model this setup we investigated two-dimensional arrays of cilia, where the cilia beat out of phase in the direction of the x axis and synchronously in the direction of the z axis. In such configurations each cilium is influenced by neighbors in the same row as well as by neighbors in the same line. If the lines of the synchronized cilia are infinite, and the cilia along these lines are equally spaced, the beat remains planar and we can still use our two-dimensional model. Liron and Mochon (1976) and later Liron (1996) proposed an efficient approach to computing the flow due to infinite lines of stokeslets in three-dimensional configurations. The implementation to our case is straightforward. Since the cilia along the line perpendicular to the plane of beating are in phase, we need only to change the singular kernels in the integral equation (Eq. 4) to account for the velocity due to identical stokeslets distributed at constant intervals on the line, and placed at the same height above the surface. The full expressions are given in detail in Liron (1996).

Fig. 4 *d* displays the sideview of the beat cycle of a single infinite line of synchronized cilia, to be compared with the beat cycle of a single cilium in panel *a*. The beat duration of the infinite line of cilia is 30 ms (frequency is 33.3 Hz), whereas the duration of a single two-dimensional cilium is 34 ms (frequency is 29.4 Hz). The beat pattern is also different: the cilia in the line are more curved during the effective stroke and less curved during the recovery stroke. The angular spread of the cilia in the infinite line is smaller than that of an isolated cilium. The upper panel of Fig. 13 displays a three-dimensional view of a semi-infinite array of 10 rows representing an infinite lines of cilia. The lower panel shows the side view of this configuration at the same time. The ciliary spacing is 1 along the lines and along the rows. The resulting beat frequency is ≈42 Hz, and some evidence for emerging phase lags can be observed. Probably, more rows are required to obtain a wavelike pattern formed by the cilia tips, but we did not simulate such configurations due to their prohibitive computational cost.

DISCUSSION

We have presented a general modeling framework for computing the forces that produce an observed ciliary beat pattern, and for fitting it into a simple plausible functional form to generate a model ciliary engine. Our engine is what we call a configuration-dependent engine, which is controlled by two geometric switches activated at the end of the effective and the recovery strokes. The modeling assumption used here is that the engine does not change its properties in response to being slowed down by external load. A

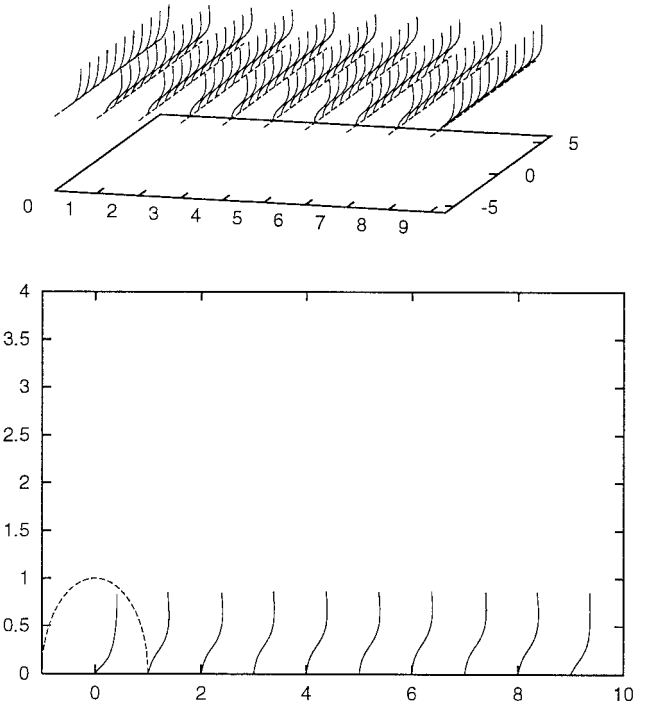

FIGURE 13 A perspective view (*upper panel*) and a side view (*lower panel*) of a semi-infinite array of cilia consisting of 10 rows, each one representing an infinite line of synchronized cilia. The snapshot is already at steady state and the beat frequency is ≈42 Hz. Small phase lags between the cilia can be observed. The spacing in the rows and in the lines is 1. The units of the axes are nondimensional length. The ellipse shown in the lower panel is the unit circle, appropriately distorted by different scaling along the horizontal and the vertical axes.

different modeling approach which would perhaps yield even a more realistic, speed-dependent engine, would include the property that dyneins generate more forces when slowed down by a load. This is an important direction for future studies.

Our model gives only a phenomenological description based on the available data. We were able to obtain surprisingly good fits to many quantitative features of the ciliary beat without getting into the details of the internal structure of the cilia. Introduction of realistic dynein-microtubule interaction kinetics and signaling control systems into the model is another important direction in which our modeling framework should be extended in the future.

The equations we use fully account for the viscous interactions between the cilia and the fluid in which they are immersed and the boundary effects. This markedly improves the accuracy and consistency of the model as compared to earlier studies. The results obtained for one cilium closely resemble the responses to changed viscosity and to externally imposed flow observed, e.g., by Sleigh (1962, 1968); Gray (1928); Okuno and Hiramoto (1976); Eshel and Gibbons (1989) and others. This demonstrates that our model engine together with the GL hydrodynamical equations capture the essential features of the problem.

With multicilia configurations, we obtained self-synchronization between two adjacent cilia. Also, the response of a single cilium to external flow fits experimental results (Gray, 1928; Okuno and Hiramoto, 1976). The results we obtained from rows of cilia and semi-infinite two-dimensional arrays of cilia indicate that metachronal-like patterns can evolve autonomously due to the hydrodynamic interaction between the cilia. This provides support for the conjecture that metachronism can, at least partially, be explained as the result of hydrodynamic coupling. Because the hydrodynamic treatment used here fully accounts for the viscous and boundary effects, and is suitable for numerical computation, a number of problems that have hitherto not been approachable are now ready to be investigated:

1. The present model demonstrates that an antiplectic metachronal wave can occur as the result of hydrodynamic interactions between neighboring cilia. Symplectic, dexioplectic, and laevoplectic metachronism also occur in nature. Such behavior could result, in principle, from an initial deformation caused by viscous interaction with adjacent cilia, which then triggers the dynein-microtubule interaction to occur in a particular direction. Work is now underway to obtain an engine and switching paradigm that would allow metachronism in any direction to evolve autonomously.
2. Our reconstruction of forces that led to the proposed model engine was based on observed beats of a supposedly single cilium. However, in most experiments, including the one whose results we used, the cilia are not isolated. Therefore, the observed beats are already the overall result of the ciliary interactions. Taking this into account while building the model for the internal engine would require more sophisticated mathematical techniques. Alternatively, we plan to apply our method to data extracted from beats of isolated cilia. Such data will hopefully be available in the near future (Z. Priel, personal communication).
3. In nature, cilia beat in three-dimensional patterns. To reach efficient functioning, the cilia are packed densely, and should be able to move freely throughout the beat phase. This is achieved by having the cilia return to their "start position" out of the plane of the effective stroke, thus creating 3-d motions, and by staggering the beat of adjacent cilia creating a metachronal wave. Gueron and Liron (1993) developed the necessary equations for modeling 3-d ciliary motion. These equations enable the propagation in time of the curvature and the torsion along a 3-d curve, given its velocity distribution. However, modeling the 3-d problem in a realistic multicilia configuration is still a formidable task. Applying our techniques and reconstructing a ciliary engine that would give a 3-d motion and possible diaplectic metachronism is a future goal.

APPENDIX

Numerical methods

For the convenience of the reader, we provide here all the details of the involved computations required for the simulations. By using this description the results reported in the paper can be reproduced.

We use $N + 1$ discretization points along the cilium, with discretization interval $ds = 1/N$. Equations 2 are integral equations with the unknowns ϕ_N and ϕ_T. We solve these equations by an iterative method and use the stopping criterion

$$\|\phi_T^{(k+1)} - \phi_T^{(k)}\|_\infty < \epsilon \quad \text{and} \quad \|\phi_N^{(k+1)} - \phi_N^{(k)}\|_\infty < \epsilon.$$

We use $\epsilon = 10^{-4}$ in our calculations.

After the drag force is computed, the values of the shear force $[F_T(s, t), F_N(s, t)]$ can be obtained from Eqs. 6. Equations 6, 13, and 15 yield a linear system of the form $Ax = b$ of $2N + 2$ unknowns, where

$$A = \left[\begin{array}{ccccccc|ccccccc} -1 & 1 & 0 & 0 & 0 & \cdots & 0 & 0 & 0 & 0 & 0 & 0 & \cdots & 0 \\ -1 & 0 & 1 & 0 & 0 & \cdots & 0 & 0 & \alpha_0 - \alpha_2 & 0 & 0 & 0 & \cdots & 0 \\ 0 & -1 & 0 & 1 & 0 & \cdots & 0 & 0 & 0 & \alpha_1 - \alpha_3 & 0 & 0 & \cdots & 0 \\ 0 & 0 & -1 & 0 & 1 & \cdots & 0 & 0 & 0 & 0 & \alpha_2 - \alpha_4 & 0 & \cdots & 0 \\ \vdots & & & \ddots & \ddots & \ddots & & \vdots & \vdots & & & \ddots & & \\ 0 & 0 & 0 & 0 & 0 & \cdots & 1 & 0 & 0 & 0 & 0 & 0 & \cdots & 0 \\ \hline 0 & 0 & 0 & 0 & 0 & \cdots & 0 & -1 & 1 & 0 & 0 & 0 & \cdots & 0 \\ 0 & \alpha_2 - \alpha_0 & 0 & 0 & 0 & \cdots & 0 & -1 & 0 & 1 & 0 & 0 & \cdots & 0 \\ 0 & 0 & \alpha_3 - \alpha_1 & 0 & 0 & \cdots & 0 & 0 & -1 & 0 & 1 & 0 & \cdots & 0 \\ 0 & 0 & 0 & \alpha_4 - \alpha_2 & 0 & \cdots & 0 & 0 & 0 & -1 & 0 & 1 & \cdots & 0 \\ \vdots & \vdots & & & \ddots & & & \vdots & & & \ddots & \ddots & \ddots & \\ 0 & 0 & 0 & 0 & 0 & \cdots & 0 & 0 & 0 & 0 & 0 & 0 & \cdots & 1 \end{array}\right] \tag{A1}$$

and

$$x^{\mathrm{T}} = [F_{\mathrm{T}_0}, F_{\mathrm{T}_1}, F_{\mathrm{T}_2}, \ldots, F_{\mathrm{T}_N} | F_{\mathrm{N}_0}, F_{\mathrm{N}_1}, F_{\mathrm{N}_2}, \ldots, F_{\mathrm{N}_N},], \tag{A2}$$

$$b^{\mathrm{T}} = [0, 2ds\phi_{\mathrm{T}_1}, 2ds\phi_{\mathrm{T}_2}, \ldots, 0 | 0, 2ds\phi_{\mathrm{N}_1}, 2ds\phi_{\mathrm{N}_2}, \ldots, 0].$$

Here F_{T_i}, F_{N_i}, ϕ_{T_i}, ϕ_{N_i} ($i = 0 \ldots N$) represent values at the discretization points.

The solution of this system gives the values of F_{T} and F_{N} at the discretization points. The values of the active shear force at these points are approximated to order $O(ds^2)$ by

$$S_i = F_{\mathrm{N}_i} - E_b \cdot \frac{(\alpha_{i+1} - 2\alpha_i + \alpha_{i-1})}{ds^2}, \qquad i = 0, 1, \ldots, N. \tag{A3}$$

If the shape of the cilium $\alpha(s, t)$ is given at time t, and the active shear force $S(s, t)$ is known, $F_{\mathrm{N}}(s, t)$ can be obtained from Eq. 11, and then $F_{\mathrm{T}}(s, t)$ can be obtained from Eq. 9. Equation 6 gives the value of the drag force $[\phi_{\mathrm{T}}(s, t), \phi_{\mathrm{N}}(s, t)]$. Using these values in Eq. 4 gives the value of $g_{\mathrm{T}}(s, t)$ and $g_{\mathrm{N}}(s, t)$. We perform this process iteratively until the stopping criteria are satisfied. Equation 9 is a second-order ordinary equation for F_{T}. The above discretization reduces it to a linear system of the form $Ax = b$ with $N + 1$ equations, where

$$A = \begin{bmatrix} -1 & 1 & 0 & 0 & \cdots & 0 \\ 1 & -2 + D_2 & 1 & 0 & \cdots & 0 \\ 0 & 1 & -2 + D_3 & 1 & \cdots & 0 \\ \vdots & & \ddots & \ddots & \ddots & \vdots \\ 0 & \cdots & 0 & 1 & -2 + D_{N-1} & 1 \\ 0 & \cdots & 0 & 0 & 0 & 1 \end{bmatrix} \tag{A4}$$

$$x^{\mathrm{T}} = [F_{\mathrm{T}_0}, F_{\mathrm{T}_1}, F_{\mathrm{T}_2}, \ldots, F_{\mathrm{T}_{N-1}}, F_{\mathrm{T}_N}], \tag{A5}$$

$$b^{\mathrm{T}} = [0, \mathrm{RHS}_1, \mathrm{RHS}_2, \ldots, \mathrm{RHS}_{N-1}, 0],$$

and, for $i = 1 \ldots N - 1$,

$$D_i = -\frac{1}{4} \cdot \frac{C_{\mathrm{T}}}{C_{\mathrm{N}}} \cdot (\alpha_{i+1} - \alpha_{i-1})^2, \tag{A6}$$

$$\mathrm{RHS}_i = \frac{1}{4}\left(1 + \frac{C_{\mathrm{T}}}{C_{\mathrm{N}}}\right) \cdot (F_{\mathrm{N}_{i+1}} - F_{\mathrm{N}_{i-1}}) \cdot (\alpha_{i+1} - \alpha_{i-1}) + F_{\mathrm{N}_i} \cdot (\alpha_{i+1} - 2\alpha_i + \alpha_{i-1}) - \frac{ds}{2} \cdot \frac{C_{\mathrm{T}}}{C_{\mathrm{N}}} \cdot g_{\mathrm{N}_i} \cdot (\alpha_{i+1} - \alpha_{i-1}) + \frac{ds}{2} \cdot (g_{\mathrm{T}_{i+1}} - g_{\mathrm{T}_{i-1}}), \tag{A7}$$

Finally, $\alpha(s, t)$ is propagated in time by solving Eq. 10, which is a nonlinear PDE for α with a fourth-order space derivative. We solve it by the Crank-Nicolson method, that is, calculating the value of α at the time $t + (dt/2)$, and repeating the above process until stopping criterion is satisfied. The discretization reduces Eq. 10 to a linear system $Ax = b$ with $N + 1$ equations, where:

$$A = \begin{bmatrix} -1 & 1 & 0 & 0 & 0 & 0 & \cdots & 0 \\ -1 & 3 & -3 & 1 & 0 & 0 & \cdots & 0 \\ L_{2_2} & L_{1_2} & D_2 & U_{1_2} & U_{2_2} & 0 & \cdots & 0 \\ 0 & L_{2_3} & L_{1_3} & D_3 & U_{1_3} & U_{2_3} & \cdots & 0 \\ \vdots & & \ddots & \ddots & \ddots & \ddots & \ddots & \\ 0 & \cdots & 0 & L_{2_{N-2}} & L_{1_{N-2}} & D_{N-2} & U_{1_{N-2}} & U_{2_{N-2}} \\ 0 & \cdots & 0 & 0 & 0 & 1 & -2 & 1 \\ 0 & \cdots & 0 & 0 & 0 & 0 & -1 & 1 \end{bmatrix} \tag{A8}$$

$$x^{\mathrm{T}} = [\alpha_0, \alpha_1, \alpha_2, \alpha_3, \ldots, \alpha_{N-2}, \alpha_{N-1}, \alpha_N],$$

$$b^{\mathrm{T}} = \left[0, -ds^2 \cdot \frac{S_0 L^2}{E_b} \cdot (S_1 - S_0), \mathrm{RHS}_2, \mathrm{RHS}_3, \ldots, \mathrm{RHS}_{N-2}, 0, 0\right], \tag{A9}$$

and, for $i = 3, 4, \ldots, N - 2$.

$$L_{2_i} = U_{2_i} = \frac{E_b}{S_0 L^2}, \tag{A10}$$

$$L_{1_i} = -4 \cdot \frac{E_b}{S_0 L^2} - \frac{ds^2}{4} \cdot \left(1 + \frac{C_{\mathrm{N}}}{C_{\mathrm{T}}}\right) \cdot (F_{\mathrm{T}_{i+1}} - F_{\mathrm{T}_{i-1}}) + ds^2 \cdot F_{\mathrm{T}_i} - \frac{1}{4} \cdot \frac{C_{\mathrm{N}}}{C_{\mathrm{T}}} \cdot \frac{E_b}{S_0 L^2} \cdot (\alpha_{i+1} - \alpha_{i-1})^2 + \frac{ds^3}{2} \cdot \frac{C_{\mathrm{N}}}{C_{\mathrm{T}}} \cdot g_{\mathrm{T}_i},$$

$$D_i = 6 \cdot \frac{E_b}{S_0 L^2} - 2 \cdot ds^2 \cdot F_{\mathrm{T}_i} + 2 \cdot \frac{ds^4}{dt} \cdot \frac{C_{\mathrm{N}} w L^2}{S_0} + 2 \cdot \frac{C_{\mathrm{N}}}{C_{\mathrm{T}}} \cdot \frac{E_b}{S_0 L^2} \cdot (\alpha_{i+1} - \alpha_{i-1})^2 \tag{A11}$$

$$U_{l_i} = -4 \cdot \frac{E_b}{S_0 L^2} + \frac{ds^2}{4} \cdot \left(1 + \frac{C_N}{C_T}\right) \cdot (F_{T_{i+1}} - F_{T_{i-1}}) + ds^2 F_{T_i}$$

$$- \frac{1}{4} \cdot \frac{C_N}{C_T} \cdot \frac{E_b}{S_0 L^2} \cdot (\alpha_{i+1} - \alpha_{i-1})^2 - \frac{ds^3}{2} \cdot \frac{C_N}{C_T} \cdot g_{T_i},$$

$$\mathrm{RHS}_i = 2 \cdot \frac{ds^4}{dt} \cdot \frac{C_N w L^2}{S_0} \cdot \alpha_i(t)$$

$$+ \frac{ds^2}{4} \cdot \frac{C_N}{C_T} \cdot S_i \cdot (\alpha_{i+1} - \alpha_{i-1})^2$$

$$+ \frac{ds^3}{2} \cdot (g_{N_{i+1}} - g_{N_{i-1}}) - ds^2 \cdot (S_{i+1} - 2S_i + S_{i-1}),$$

After the values of $\alpha(s, t)$ and $\alpha[s, t + (dt/2)]$ are computed, we obtain the value of $\alpha(s, t + dt)$ by

$$\alpha(s, t + dt) \approx 2 \cdot \alpha\left(s, t + \frac{dt}{2}\right) - \alpha(s, t) + O(dt).$$

Finally, note that for clarity the calculation procedure is displayed as a flow chart in Fig. 1. Similarly to the result reported by Hines and Blum (1978) and by Gueron and Liron (1992) we found that the stopping criterion is satisfied already after five iterations.

The complexity of the simulation algorithm is $O(P^2N^2)$ where P is the number of the simulated cilia and N is the number of discretization points along each cilium. Hence, simulations of large multicilia configurations are a heavy computational task. Although modern computer technology enables us to run simulations of large multicilia arrays, practical limitations still exist. For example, the simulation of a 100-cilia configuration for 5 cycles (1200 time steps) takes ~400 CPU hours. All calculations and simulations reported in with work were performed on SUN SPARC 10 workstation.

We thank Prof. Nadav Liron from the Department of Mathematics at the Technion and Prof. Jacob J. Blum from the Department of Cell Biology at Duke University Medical Center for many helpful discussions and for their active help during the preparation of the paper. We also thank an anonymous referee for a very thorough review with many valuable suggestions.

This research was supported by the U.S.–Israel Binational Science Foundation Grant 94-242, by the Technion V.P.R. fund, and by the Fund for the Promotion of Research at the Technion. S. Gueron acknowledges the support of the Henri Gutwirth Fund for the Promotion of Research.

REFERENCES

Blake, J. 1972. A model for the micro-structure in ciliated organisms. *J. Fluid Mech.* 55:1–23.

Blum, J. J., and M. Hines. 1979. Biophysics of flagellar motility. *Rev. Biophys. Quarterly.* 12:103–180.

Brennen, C., and H. Winet. 1977. Fluid mechanics of propulsion by cilia and flagella. *Annu. Rev. Fluid. Mech.* 9:339–398.

Brokaw, C. J. 1972. Computer simulation of flagellar movement. I. demonstration of stable bend propagation and bend initiation by the sliding filament model. *Biophys. J.* 12:564–586.

Brokaw, C. J. 1985. Computer simulation of flagellar movement. VI. simple curvature-controlled models are incompletely specified. *Biophys. J.* 48:633–642.

Childress, S. 1981. Mechanics of Swimming and Flying. Cambridge University Press, Cambridge.

Dresdner, R. D., D. F. Katz, and S. A. Berger. 1980. The propulsion by large amplitude waves of uniflagellar micro-organisms of finite length. *J. Fluid Mech.* 97:591–621.

Ermentrout, G. B. 1985. The behavior of rings of coupled oscillators. *J. Math. Biol.* 23:55–74.

Ermentrout, G. B., and N. Kopell. 1984. Frequency plateaus in a chain of weakly coupled oscillators I. *SIAM. J. Math. Anal.* 15:215–237.

Eshel, D., and I. R. Gibbons. 1989. External mechanical control of the timing of bend initiation in sea urchin sperm flagella. *Cell Motil. Cytoskeleton.* 14:416–423.

Gheber, L., and Z. Priel. 1989. Synchronization between beating cilia. *Biophys. J.* 55:183–191.

Gray, J. 1928. Ciliary Movement. Cambridge University Press, Cambridge.

Gray, J., and G. Hancock. 1955. The propulsion of sea-urchin spermatozoa. *J. Exp. Biol.* 32:802–814.

Gueron, S., K. Levit-Gurevich, N. Liron, and J. J. Blum. 1997. Cilia internal mechanism and metachronal coordination as the result of hydrodynamical coupling. *Proc. Natl. Acad. Sci. USA* 94:6001–6006.

Gueron, S., and N. Liron. 1992. Ciliary motion modeling, and dynamic multicilia interactions. *Biophys. J.* 63:1045–1058.

Gueron, S., and N. Liron. 1993. Simulations of three-dimensional ciliary beats and cilia interactions. *Biophys. J.* 65:499–507.

Higdon, J. J. L. 1979a. A hydrodynamic analysis of flagellar propulsion. *J. Fluid Mech.* 90:685–711.

Higdon, J. J. L. 1979b. The generation of feeding currents by flagellar motion. *J. Fluid Mech.* 94:305–330.

Higdon, J. J. L. 1979c. The hydrodynamics of flagellar propulsion: helical waves. *J. Fluid Mech.* 94:331–351.

Hines, M., and J. J. Blum. 1978. Bend propagation in flagella. I. Derivation of equations of motion and their simulation. *Biophys. J.* 23:41–57.

Hines, M., and J. J. Blum. 1979. Bend propagation in flagella. II. Incorporation of dynein cross-bridge kinetics into the equations of motion. *Biophys. J.* 25:421–442.

Johnson, R. E., and C. J. Brokaw. 1979. Flagellar hydrodynamics: a comparison between resistive-force theory and slender-body theory. *Biophys. J.* 25:113–127.

Lighthill, J. L. 1975. Mathematical Biofluiddynamics. Regional Conference Series in Applied Mathematics. SIAM, Philadelphia. 45–62.

Lighthill, J. L. 1976. Flagellar hydrodynamics. *SIAM Rev.* 18:161–230.

Liron, N. 1996. Stokes flow due to infinite arrays of stokeslets in three dimensions. *J. Eng. Math.* 30:267–297.

Liron, N., and S. Mochon. 1976. The discrete-cilia approach for propulsion of ciliated microorganisms. *J. Fluid Mech.* 75:593–607.

Lubliner, J. 1973. An analysis of interfilament shear in flagella. *J. Theor. Biol.* 41:119–125.

Machemer, H. 1972. Ciliary activity and the origin of metachronism in paramecium: effects of increased viscosity. *J. Exp. Biol.* 57:239–259.

Machin, M. E. 1963. The control and synchronization of flagellar movement. *Proc. R. Soc. Lond. B.* 158:88–104.

Murase, M. 1990. Simulation of ciliary beating by an excitable dynein model: oscillations, quiescence and mechano-sensitivity. *J. Theor. Biol.* 146:209–231.

Murase, M. 1991. Excitable dynein model with multiple active sites for large-amplitude oscillations and bend propagation in flagella. *J. Theor. Biol.* 149:181–202.

Murase, M. 1992. Dynamics of Cellular Motility. John Wiley & Sons Ltd., New York.

Murase, M., M. Hines, and J. J. Blum. 1989. Properties of an excitable dynein model for bend propagation in cilia and flagella. *J. Theor. Biol.* 139:413–430.

Murase, M., and H. Shimizu. 1986. A model of flagellar movement based on cooperative dynamics of dynein-tubulin cross-bridges. *J. Theor. Biol.* 119:409–433.

Myerscough, M. R., and M. A. Swan. 1989. A model for swimming unipolar spirilla. *J. Theor. Biol.* 139:201–218.

Okuno, O., and Y. Hiramoto. 1976. Mechanical simulation of starfish flagella. *J. Exp. Biol.* 65:401–413.

Phan-Thien, N., T. Tran-Cong, and M. Ramia. 1987. A boundary-element analysis of flagellar propulsion. *J. Fluid Mech.* 185:533–549.

Ramia, M. 1991. Numerical model or the locomotion of spirilla. *Biophys. J.* 60:1057–1078.

Satir, P. 1985. Switching mechanisms in the control of ciliary motility. *Mol. Cell. Biol.* 4:1–46.

Sleigh, M. A. 1962. The Biology of Cilia and Flagella. Pergamon Press, Oxford.

Sleigh, M. A. 1968. Patterns of ciliary beating. *Aspects of Cell Motility (22nd Symposium of the Society for Experimental Biology)*. P. L. Miller, editor. 131–150.

Sleigh, M. A. 1974. Metachronism of cilia of Metazoa. *In* Cilia and Flagella. M. A. Sleigh, editor. Academic Press, London. 287–304.

Sleigh, M. A., and D. I. Barlow. 1982. How are different ciliary beat patterns produced? *Symposia of the Society for Experimental Biology*. 35:139–157.

Tamm, S. L. 1972. Ciliary motion in Paramecium. *J. Cell Biol.* 55: 250–255.